Plant-derived exosome-like nanovesicles improve testicular injury by alleviating cell cycle arrest in Sertoli cells

Yong Jiang

yongjiang@bjmu.edu.cn

Peking University

Xiao Zhang

Peking University

Yuling xiao

Peking university

Xingzi Hou

Peking university

Chenlong Wei

School of Pharmaceutical Sciences, Peking University

Meng Ding

Peking university

Wangxiao Tan

Peking university

Peng-Fei Tu

Peking University https://orcid.org/0000-0002-3848-8174

Article

Keywords:

Posted Date: November 17th, 2025

DOI: https://doi.org/10.21203/rs.3.rs-8050231/v1

Additional Declarations: There is **NO** Competing Interest.

Plant-derived exosome-like nanovesicles improve testicular injury by alleviating cell cycle arrest in Sertoli cells

Yuling Xiao, Xingzi Hou, Chenlong Wei, Meng Ding, Wangxiao Tan, Pengfei Tu, Xiao Zhang*, and Yong Jiang*

State Key Laboratory of Natural and Biomimetic Drugs, School of Pharmaceutical Sciences, Peking University, Beijing 100191, China

*Corresponding authors.

E-mail addresses: yongjiang@bjmu.edu.cn (Yong Jiang), xiao_zhang@bjmu.edu.cn (Xiao Zhang).

Abstract

The testis plays a vital role in male reproduction, and its function directly impacts spermatogenesis and male fertility. Cyclophosphamide, a commonly used chemotherapeutic agent, induces severe testicular toxicity; however, effective strategies for prevention or treatment are currently lacking. In this study, we isolated and identified exosome-like nanovesicles derived from *Cistanche deserticola* (CDELNs), characterized their composition, and investigated their therapeutic effects and molecular mechanisms on cyclophosphamide-induced testicular injury. Specifically, we found that CDELNs are preferentially taken up by testicular Sertoli cells, and this uptake process is mediated by heparan sulfate proteoglycans (HSPG). Mechanistically, miR159b-3p derived from CDELNs alleviates cell cycle arrest and restores testicular function by inhibiting the expression of the cell cycle inhibitor P21, thereby promoting the phosphorylation-dependent activation of cyclin-dependent kinase 1 (CDK1). Furthermore, single-cell transcriptomic analysis of testicular tissues from patients with non-obstructive azoospermia (NOA) in published database revealed that Sertoli cells and P21 are critically involved in male reproductive disorders, suggesting that CDELNs-based intervention strategy targeting P21 holds broad prospects for clinical translation. Collectively, our study reveals firstly that CDELNs, a novel bioactive substrate of *Cistanche deserticola*, exert therapeutic effects on male testicular injury by regulating the cell cycle pathway through their miRNA.

Introduction

The testis is essential for male reproductive health, playing a critical role in both spermatogenesis and androgen synthesis[1,2]. With the increasing incidence of tumors in modern society, the application of chemotherapeutic agents in cancer treatment has become more prevalent; among these, cyclophosphamide is one of the most widely used chemotherapeutics in clinical practice[3]. However, the reproductive toxicity of cyclophosphamide has also attracted widespread concern[4–6]. Cyclophosphamide can induce inhibition of testicular cell proliferation and damage to spermatogenic function,

leading to reduced sperm quality and quantity, and may even affect fertility and the growth and development of offspring[7,8]. Therefore, in-depth exploration of the mechanisms underlying cyclophosphamide-induced testicular injury and search for effective intervention strategies hold significant clinical importance.

Testicular injury involves multi-level pathological changes in both germ cells and somatic cells[9]. Research indicates that cyclophosphamide exposure results in a significant reduction in the number of testicular spermatogonia and spermatocytes, accompanied by the accumulation of DNA damage and gene mutations in germ cells[10,11]. As key somatic cells that provide structural support and nutrients within the seminiferous tubules, Sertoli cells are also highly susceptible to chemotherapeutic agents[12–14]. Cyclophosphamide has been demonstrated to trigger the generation of reactive oxygen species (ROS) and promote the process of lipid peroxidation, causing vacuolation, numerical reduction, structural destruction, and secretory dysfunction of Sertoli cells. Ultimately, this leads to Sertoli cell inactivation and subsequent spermatogenic disorders[15–17]. Nevertheless, systematic analysis of transcriptomic changes and molecular mechanisms during testicular injury remains insufficient. Meanwhile, there is a severe lack of drugs to alleviate or treat reproductive damage caused by chemotherapeutic agents such as cyclophosphamide.

Plant-derived exosome-like nanovesicles (PELNs) possess a lipid bilayer structure, containing proteins, lipids, nucleic acids, and bioactive small molecules[18–20]. Owing to their natural origin, sustainable high-yield potential, low immunogenicity, and good tolerance by mammalian cells, PELNs exhibit the potential to deliver bioactive molecules across species and exert therapeutic effects[21,22]. Recent studies have demonstrated that PELNs derived from plants such as ginseng[23], ginger[24], and platycodon grandiflorum[25], can significantly alleviate inflammation[26], inhibit tumor growth[27], and improve metabolic diseases[28,29]. Despite the therapeutic potential of PELNs in various disease models, their role in male reproductive protection has not been reported to date.

Cistanche deserticola is a valuable traditional Chinese medicinal herb with both medicinal and edible properties, known as the “ginseng of the desert”[30]. As a root-

parasitic plant, it parasitizes the roots of *Haloxylon ammodendron*, a plant that stabilizes sand dunes and prevents desertification[31]. Thus, the research and development of *C. deserticola* are not only of great significance to the health industry but also hold important social value for promoting local ecological management. *C. deserticola* has the traditional efficacy of "tonifying the kidney and replenishing essence". It is commonly used to improve sexual function and treat male reproductive disorders such as oligoasthenospermia and erectile dysfunction, with a long history of application in Asian countries[32]. Traditionally, its small-molecule components (e.g., phenylethanoid glycosides) have been used for the treatment of reproductive diseases[33,34], while reports about its nanovesicles are absent. In this study, we isolated and purified exosome-like nanovesicles from *C. deserticola* (CDELNs) using differential centrifugation combined with sucrose density gradient centrifugation. The morphology, particle size distribution, surface charge, and molecular composition of these nanovesicles were systematically characterized via transmission electron microscopy, particle size analysis, zeta potential measurement, and multi-omics integration analysis (proteomics, transcriptomics, and lipidomics). Meanwhile, *in vitro* and *in vivo* experiments revealed that CDELNs can act as a natural nanoplatform to deliver intrinsic functional miRNAs. By alleviating cell cycle arrest in testicular Sertoli cells and restoring their physiological functions, CDELNs significantly improve cyclophosphamide-induced testicular injury and spermatogenic dysfunction.

Results

Isolation and Characterization of CDELNs

CDELNs were isolated from the fresh fleshy stems of *Cistanche deserticola* collected from Turpan, Xinjiang, using differential centrifugation combined with sucrose density gradient centrifugation (Fig. 1A). Sucrose gradient centrifugation showed that CDELNs primarily sedimented at the 30%–45% interface. The morphology of CDELNs was characterized by transmission electron microscopy (TEM), which revealed that CDELNs exhibited a typical spherical nanovesicle structure (Fig. 1B).

Nanoparticle tracking analysis (NTA) demonstrated that the purified CDELNs had an average particle size of approximately 168.6 nm (Fig. 1B). Zeta potential measurements revealed that CDELNs possessed a surface charge of –28.7 mV (Fig. 1C); zeta potential is a critical parameter for evaluating the stability of nanoparticles, and a higher absolute value predicts good stability in aqueous dispersions, effectively preventing spontaneous aggregation between particles[35]. The polydispersity index (PDI) of the CDELNs solution was < 0.2, indicating that CDELNs had a concentrated particle size distribution and good homogeneity, which is favorable for *in vivo* studies (Fig. 1D). Bicinchoninic acid (BCA) assay showed that approximately 2.1 mg of CELN protein could be obtained per kilogram of fresh *C. deserticola* (Supplementary Fig. 1A), confirming that this medicinal plant can be used for efficient acquisition of nanovesicles. When comparing different storage conditions, CDELNs were found to be stably stored at –80°C, with no significant changes in morphology and particle size after one month (Supplementary Fig. 1B–D). Furthermore, to investigate the universality of the isolation method and the influence of raw material sources, we further compared fresh *C. deserticola* samples from different geographical origins (Alxa League, Inner Mongolia; Baiyin City, Gansu Province) and aqueous extracts of traditionally processed herbal slices. The results showed that CDELNs could be successfully isolated from fresh samples of all geographical origins, although there were slight differences in their particle size distributions. Numerous vesicular structures were also observed in samples prepared by the traditional aqueous decoction process, with a small number of vesicles showing rupture (Supplementary Fig. 1E).

Plant-derived exosome-like nanovesicles typically contain multiple components, including lipids, proteins, nucleic acids, and various bioactive small molecules[21,36]. Previous studies have reported that phenylethanoid glycosides (e.g., echinacoside), major bioactive components of *C. deserticola*, exhibit anti-reproductive injury activity, which can effectively restore sperm count and motility, increase luteinizing hormone and testosterone levels, and alleviate sperm damage[37,38]. However, liquid chromatography-tandem mass spectrometry (LC-MS/MS) analysis of small molecules revealed that the main small-molecule compounds in CDELNs were betaine (peak area

ratio: 26.9%), malate (11.62%) and choline (6.63%), while the content of phenylethanoid glycosides was extremely low (0.03%) (Fig. 1E). This suggests that CDELNs may exert their functions through other components.

Lipidomic analysis revealed that CDELNs were enriched in glycerolipids (GL: 41.19%), glycerophospholipids (GP: 29.51%), and fatty acyls (FA: 17.99%), mainly including diglycerides (DG), *N*-acylethanolamines (NAE), and phosphatidylcholines (PC) (Fig. 1F, G). According to previous reports, glycerolipids can alter membrane curvature and fluidity, promoting the formation and release of CDELNs[39]. As the major phospholipid component of cell membranes, phosphatidylcholines contribute to maintaining the integrity and stability of the CDELNs membrane[40].

Proteomic analysis identified 987 proteins in CDELNs (Supplementary Fig. 1F), including plasma membrane-associated proteins (e.g., aquaporins PIP1-3/PIP1-4), key proteins involved in metabolic processes (e.g., ATP synthase), proteins related to protein folding and processing (e.g., chaperones CPN60), and ribosomal proteins (e.g., ubiquitin-S27a). Additionally, heat shock proteins 70 and 90, frequently reported in exosome studies, were also detected[41]. Gene Ontology (GO) enrichment analysis categorized these proteins into three major classes: biological processes, cellular components, and molecular functions (Fig. 1H), revealing that CDELNs-contained proteins exhibit diverse biological functions, varied cellular localizations, and participate in multiple biological regulatory processes. Kyoto Encyclopedia of Genes and Genomes (KEGG) enrichment analysis further showed that the main regulated pathways included glycolysis/gluconeogenesis, pyruvate metabolism, histidine metabolism, β-alanine metabolism, and tryptophan metabolism (Fig. 1I).

Exosomes are also rich in nucleic acids. Transcriptomic analysis of mRNAs in CDELNs identified 35,272 genes. GO enrichment analysis revealed that these genes in CDELNs exhibit diverse biological functions, varied cellular localizations, and participate in multiple biological regulatory processes, including cellular macromolecular metabolic processes, biosynthetic processes, and actin polymerization or depolymerization processes (Fig. 1J). KEGG pathway enrichment analysis showed

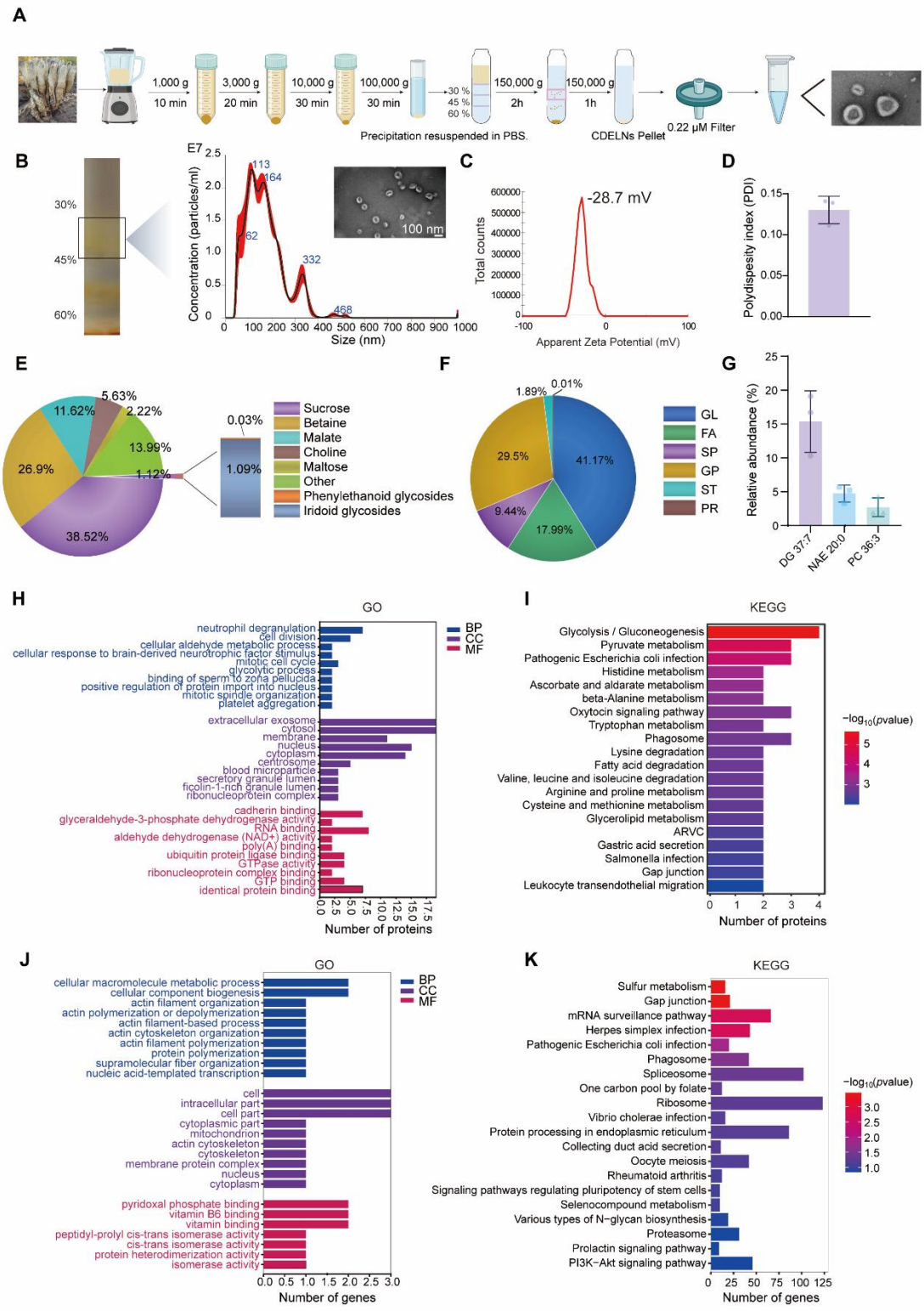

Fig. 1 | Identification and characterization of CDELNs. A Schematic of the preparation process of CDELNs. **B** TEM images and size distribution from 30%/45% interface of sucrose gradient solution. **C, D** Zeta potential (**C**) and PDI (**D**) of CDELNs by dynamic light scattering (DLS). Data are presented as the means ± SDs. *n* = 3 biological replicates. **E, F** Small molecule metabolites (**E**)

and lipids (**F**) in CDELNs by LC-MS/MS. **H, I** GO (**H**) and KEGG pathway (**I**) enrichment analysis of proteins in CDELNs. **J, K** GO (**J**) and KEGG pathway (**K**) enrichment analysis of mRNAs in CDELNs.

that the main regulated pathways were sulfur metabolism and gap junctions (Fig. 1K). This suggests that CDELNs may enhance the antioxidant stress capacity of recipient cells by delivering sulfur metabolism-related factors, and maintain intercellular communication and structural integrity by regulating gap junctions and the actin cytoskeleton, thereby synergistically improving the physiological functions of recipient cells[42–44]. Collectively, these results demonstrate that CDELNs are enriched with small-molecule metabolites, lipids, proteins, and nucleic acids.

Cellular uptake and stability of CDELNs *in vitro*

Cellular uptake is an essential prerequisite for plant-derived exosome-like nanovesicles to deliver their bioactive cargo and subsequently mediate intended therapeutic outcomes. In this study, we investigated the uptake of CDELNs by four types of testicular cells. First, we assessed the cytotoxicity of CDELNs against GC1 spermatogonia cells, GC2 spermatocyte cells, TM3 Leydig cells, and TM4 Sertoli cells. CDELNs exhibited no cytotoxicity toward these cells and even promoted cell viability within 25 μg/mL, which was selected for subsequent experiments (Supplementary Fig. 2A). Next, these cells were co-incubated with DiD-labeled CDELNs. Long time-lapse imaging showed that CDELNs could be taken up by all these testicular cell types, with significantly higher uptake efficiency in TM4 Sertoli cells (Supplementary Fig. 2B, C). The differential uptake efficiency of CDELNs among these cells may be attributed to the heterogeneity of their surface receptors. Fluorescence microscopic imaging revealed that CDELNs were mainly localized in the cytoplasm of TM4 cells (Fig. 2A). Flow cytometry analysis demonstrated that TM4 cells continuously and efficiently took up CDELNs in a time-dependent manner, with the percentage of CDELNs-containing cells increasing from 34% at 3 h to 98% at 24 h (Fig. 2B, C). To further clarify the internalization mechanism of CDELNs by TM4 cells, cells were treated with appro-

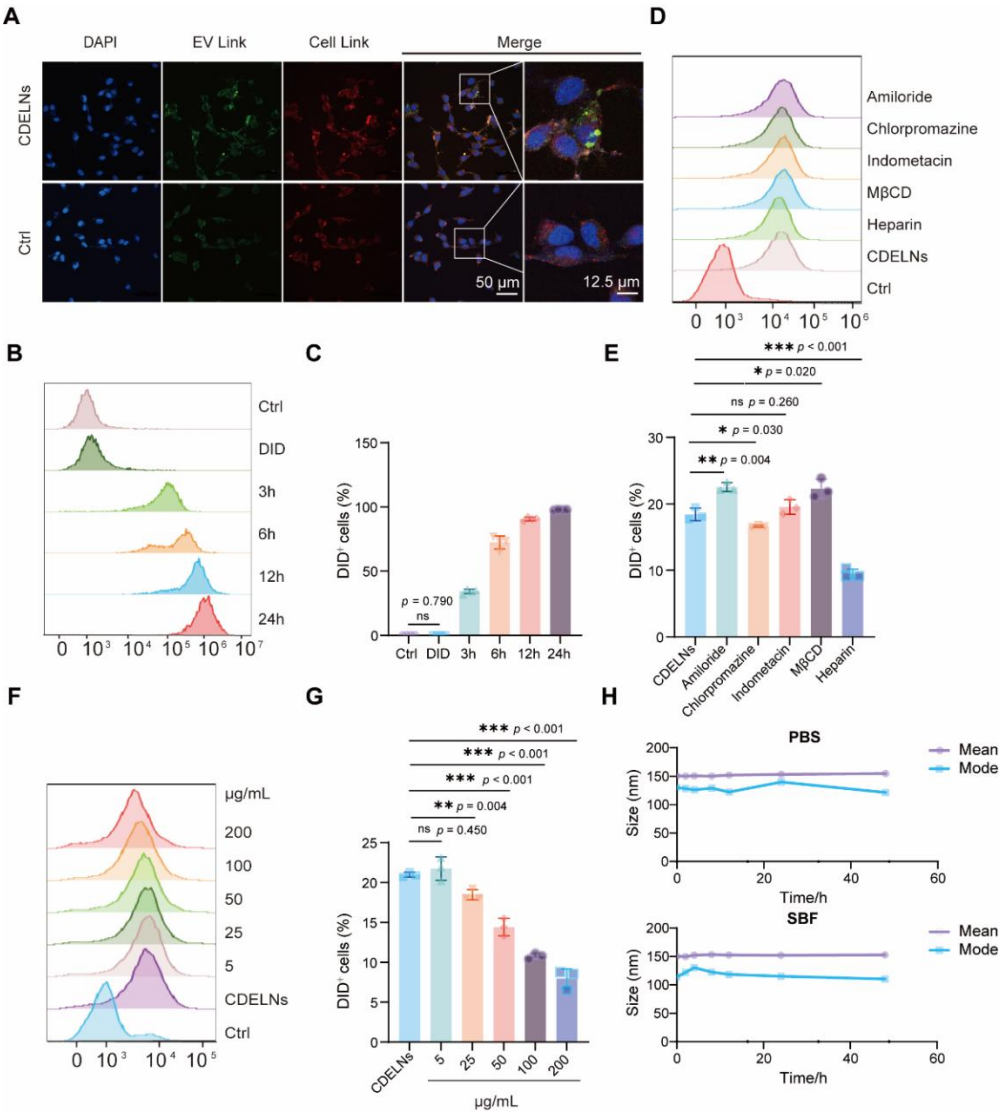

Fig. 2 | Cellular uptake and stability of CDELNs *in vitro*. A Representative confocal image of TM4 cells treated with CDELNs or Vehicle. CDELNs and cell membrane were stained with EV link (green) and Cell link (red). **B** Flow cytometric analysis of TM4 cells treated with DiD-CDELNs for different time. **C** Quantitative analysis of DiD-CDELNs$^+$ cells in (**B**) (n = 3). **D** Flow cytometric analysis of TM4 cells treated with different endocytosis inhibitors. **E** Quantitative analysis of DiD-CDELNs$^+$ cells in (**D**) (n = 3). **F** Flow cytometric analysis of TM4 cells treated with different dose of Heparin. **G** Quantitative analysis of DiD-CDELNs$^+$ cells in (**F**) (n = 3). **H** Changes in the mean particle sizes and mode sizes of CDELNs after incubation in PBS or SBF at 37 °C for 1 h, 3 h, 6 h, 12 h, 24 h and 48 h. All data are presented as the means ± SDs.

priate concentrations of inhibitors, including amiloride (macropinocytosis inhibitor), chlorpromazine (clathrin-mediated endocytosis inhibitor), indometacin (caveolin-

mediated endocytosis inhibitor), heparin (heparan sulfate proteoglycan (HSPG)-mediated endocytosis inhibitor), and MβCD (lipid raft-mediated endocytosis inhibitor) (Supplementary Fig. 2D)[45,46]. Flow cytometry analysis showed that heparin exerted a significant inhibitory effect, reducing CELN internalization by 51.6% compared to the control group (Fig. 2D, E), and this inhibitory effect was dose-dependent (Fig. 2F, G). These findings indicate that HSPG-mediated endocytosis is the primary mechanism underlying CELN uptake by TM4 cells.

Among various administration routes, intraperitoneal injection is widely used due to its advantages: it enables rapid drug onset, is easy to operate, and has low requirements for patients. However, the complex intraperitoneal microenvironment poses considerable challenges for the intraperitoneal delivery of biomaterials. To evaluate the stability of CDELNs in the intraperitoneal cavity, CDELNs were co-incubated with phosphate-buffered saline (PBS) or simulated body fluid (SBF) for different durations. Nanoparticle tracking analysis (NTA) was used to detect changes in their particle size distribution. As shown in Fig. 2H and Supplementary Fig. 2E, the particle size of CDELNs remained stable in both PBS and SBF at all time points. These findings indicate that CDELNs can maintain their integrity for at least 48 h after entering the intraperitoneal cavity.

CDELNs ameliorate Sertoli cells injury via P21 *in vitro*

To determine whether CDELNs could promote cyclophosphamide-induced testicular cell injury, TM4 cells were treated with 4 μM 4-hydroperoxycyclophosphamide (4-HC), the active metabolite of cyclophosphamide, for 8 h, followed by treatment with CDELNs for 24 h. MTT assays showed 4-HC treatment significantly inhibited cell viability, reducing the survival rate to 59.5%. In contrast, CDELNs improved cell viability in a dose-dependent manner. The survival rates of TM4 cells treated with 6.25, 12.5 and 25 μg/mL CDELNs were 83.8%, 108.9% and 121.0%, respectively (Fig. 3A). These results suggest that CDELNs not only effectively counteract the cytotoxicity of 4-HC but may also contain bioactive components that promote cellular metabolism or proliferation, thereby further enhancing the overall viability of cells after injury repair.

Previous studies have shown that the cytotoxicity of cyclophosphamide is often closely associated with oxidative stress, DNA damage, and cell cycle arrest[47,48]. To explore the protective mechanism of CDELNs, we first detected intracellular reactive oxygen species (ROS) levels using the ROS-specific fluorescent probe DCFH-DA. Flow cytometry analysis showed that 4-HC treatment increased ROS levels, while CDELNs significantly reversed this phenomenon (Fig. 3B, C). Similarly, the same result was observed when ROS levels were detected by fluorescence microscopy (Supplementary Fig. 3A, B). Oxidative stress leads to severe DNA damage, characterized by a significant increase in the fluorescent signal of γ-H2AX, a marker of DNA double-strand breaks. Consistently, CDELNs treatment substantially reduced this signal (Fig. 3D, E). Subsequently, DNA damage activates cell cycle checkpoints, triggering proliferation arrest. Cell cycle analysis via flow cytometry revealed that 4-HC treatment induced a typical G2/M arrest, a classic cellular response to pause division for DNA repair after damage, while CDELNs intervention alleviated this cell cycle arrest (Fig. 3F, G).

The G2-M transition is primarily driven by the activation of the Cyclin-Dependent Kinase 1/Cyclin B (CDK1/CCNB) complex, whose activity can be suppressed by the cyclin-dependent kinase inhibitor p21 (CDKN1A) in response to cellular stress, such as DNA damage[49].To investigate the molecular mechanism underlying cell cycle arrest, we detected the expression levels of P21. qRT-PCR results showed that P21exhibited an expression pattern consistent with the cell cycle arrest phenotype, whose expression was significantly upregulated after 4-HC treatment and effectively reversed by CDELNs (Fig. 3H). This trend was further verified at the protein level by western blot analysis (Fig. 3I, J). Immunofluorescence staining further confirmed that the nuclear signal of P21 was markedly enhanced after 4-HC treatment, and this enhancement was efficiently reversed by CDELNs (Fig. 3K, L). Collectively, these results suggest that P21 may be a key target of CDELNs for reversing cell cycle arrest and exerting protective effects.

To directly investigate the function of P21, we overexpressed P21 in TM4 cells. MTT analysis showed that P21 overexpression alone was sufficient to reduce cell

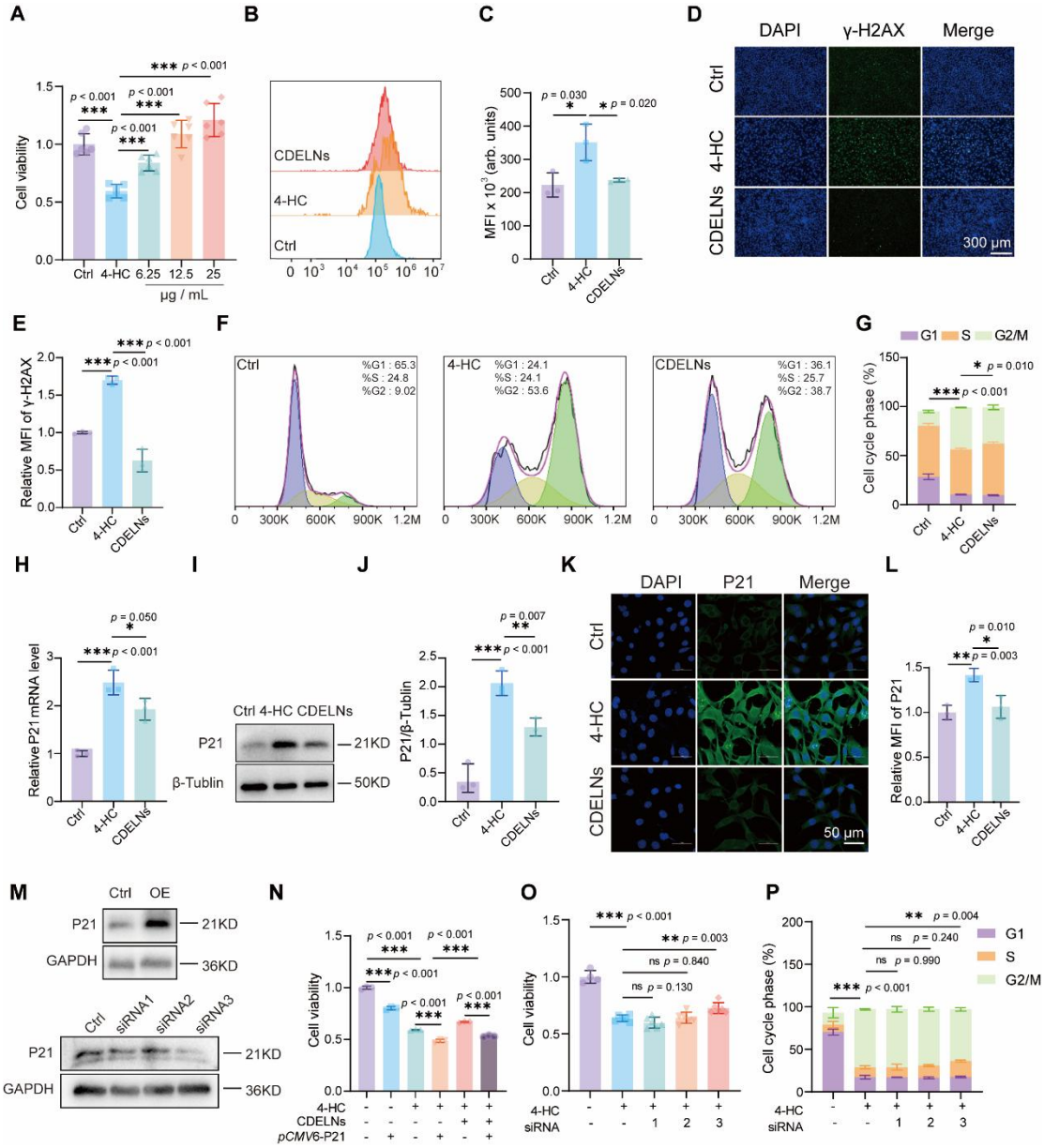

Fig. 3 | CDELNs alleviate 4-HC-induced TM4 cell damage through P21. A CDELNs increased cell viability against 4-HC induced injury in TM4 cells. **B** CDELNs reversed 4-HC induced ROS increase in TM4 cells by flow cytometric analysis. **C** Quantitative analysis of mean fluorescence intensity of ROS in (**B**) ($n = 3$). **D** Representative immunostaining images of γ-H2AX in TM4 cells. **E** Quantitative analysis of mean fluorescence intensity of γ-H2AX in (**D**) ($n = 3$). **F** CDELNs relieved 4-HC induced cell cycle arrest in TM4 cells by flow cytometric analysis. **G** Quantitative analysis of cell cycle phase in (**F**) ($n = 3$). **H** qRT-PCR analysis of P21 expression in TM4 cells. **I** Western blot analysis of P21 expression in TM4 cells. **J** Quantitative analysis of P21 expression in (**K**) ($n = 3$). **K** Representative immunostaining images of P21 in TM4 cells. **L** Quantitative analysis of mean fluorescence intensity of P21 in (**K**) ($n = 3$). **M** Western blot analysis of P21 expression in

TM4 cells transfected with *pCMV*6-P21and P21 siRNA respectively. **N** P21 overexpression reduced cell viability against 4-HC induced injury in TM4 cells (n = 3). **O** P21 knockdown increased cell viability against 4-HC induced injury in TM4 cells (n = 3). **P** P21 knockdown relieved 4-HC induced cell cycle arrest in TM4 cells by flow cytometric analysis (n = 3). All data are presented as the means ± SDs.

viability, mimicking the damaging phenotype induced by cyclophosphamide (Fig. 3M, N). More importantly, P21 overexpression significantly attenuated the protective effect of CDELNs on cell viability (Fig. 3N). This indicates that the upregulation of P21 is sufficient to counteract the beneficial effects of CDELNs, confirming P21 as a critical target for CELN-mediated functions. Conversely, knockdown of P21 in the 4-HC-induced injury model successfully recapitulated the beneficial effects of CDELNs, effectively improving cell viability and restoring cell cycle progression (Fig. 3M, O, P and Supplementary Fig. 3C). These findings demonstrate that CDELNs exert reproductive protective effects by targeting P21, establishing P21 as a potential therapeutic target for reproductive injury.

miRNAs derived from CDELNs regulate Sertoli cells viability and cell cycle

To identify the key bioactive components of CDELNs that exert reproductive protective effects, we conducted a series of component function validation experiments. First, CDELNs were heated at 98 °C for 10 min to denature proteins. Transmission electron microscopy (TEM) results showed that heat-treated CDELNs still maintained intact nanovesicle structures (Fig. 4A), and their ability to ameliorate cyclophosphamide-induced reduction in cell viability was not impaired (Fig. 4B). This ruled out the possibility that proteins in the vesicles serve as the key bioactive components. Subsequently, we evaluated the effects of the three most abundant small-molecule metabolites in CDELNs (betaine, malate, and choline). None of these metabolites could reverse the cyclophosphamide-induced decrease in cell viability, suggesting that small-molecule metabolites in the vesicles are not the bioactive components (Supplementary Fig. 4A–C). We then extracted total RNA from CDELNs and directly transfected it into

TM4 cells. MTT analysis showed that CDELNs-derived RNA was sufficient to mimic the effects of intact CDELNs, significantly alleviating cyclophosphamide-induced reductions in cell viability and cell cycle arrest. Further extraction of miRNAs from CDELNs and transfection into TM4 cells exhibited the same protective effects (Fig. 4C–E). Collectively, these results indicate that RNA in CDELNs, particularly miRNAs, are the key bioactive components mediating their reproductive protective functions.

Small RNAs are defined as short non-coding RNAs that, following their intercellular transport via extracellular vesicles, mediate sequence-specific gene silencing by binding to complementary messenger RNAs in animal systems[50–52]. To identify the key functional miRNAs in CDELNs, miRNA sequencing analysis was performed. In eukaryotes, the specific cleavage of precursor miRNAs by Dicer enzyme typically results in a strong species-conserved preference for the first base at the 5' end of mature miRNA sequences[53,54]. To explore the biological characteristics of miRNAs carried by CDELNs, we analyzed the distribution of the first base in miRNAs of different lengths and statistically examined the base distribution pattern at each position of the miRNAs. The first base at the 5' end of these miRNAs did not exhibit the typical uridine preference of plant miRNAs; instead, they showed a preference for cytosine and guanine. The position-specific base distribution map further confirmed this atypical base distribution feature at the first position (Supplementary Fig. 4D). This suggests that *C. deserticola*, as a parasitic plant, may enrich a large number of species-specific miRNAs. Based on miRNA sequencing data, with TPM > 1 as the threshold, 32 high-abundance miRNAs were screened (Fig. 4F). To identify molecules that can be efficiently taken up by mammalian cells and have potential regulatory activity, the expression profile of endogenous miRNAs was detected in TM4 cells after CELN treatment. qRT-PCR analysis showed four miRNAs with significantly upregulated expression levels were identified, including miR159b-3p, miR168a-5p, miR858b, and miR6300 (Fig. 4G). Subsequent functional validation of these four miRNAs was conducted through transfecting the corresponding miRNA mimics into TM4 cells. Three miRNAs (miR159b-3p, miR858b, and miR6300) alleviated the cyclophosphamide-induced decrease in cell viability, while miR159b-3p, miR168a-5p,

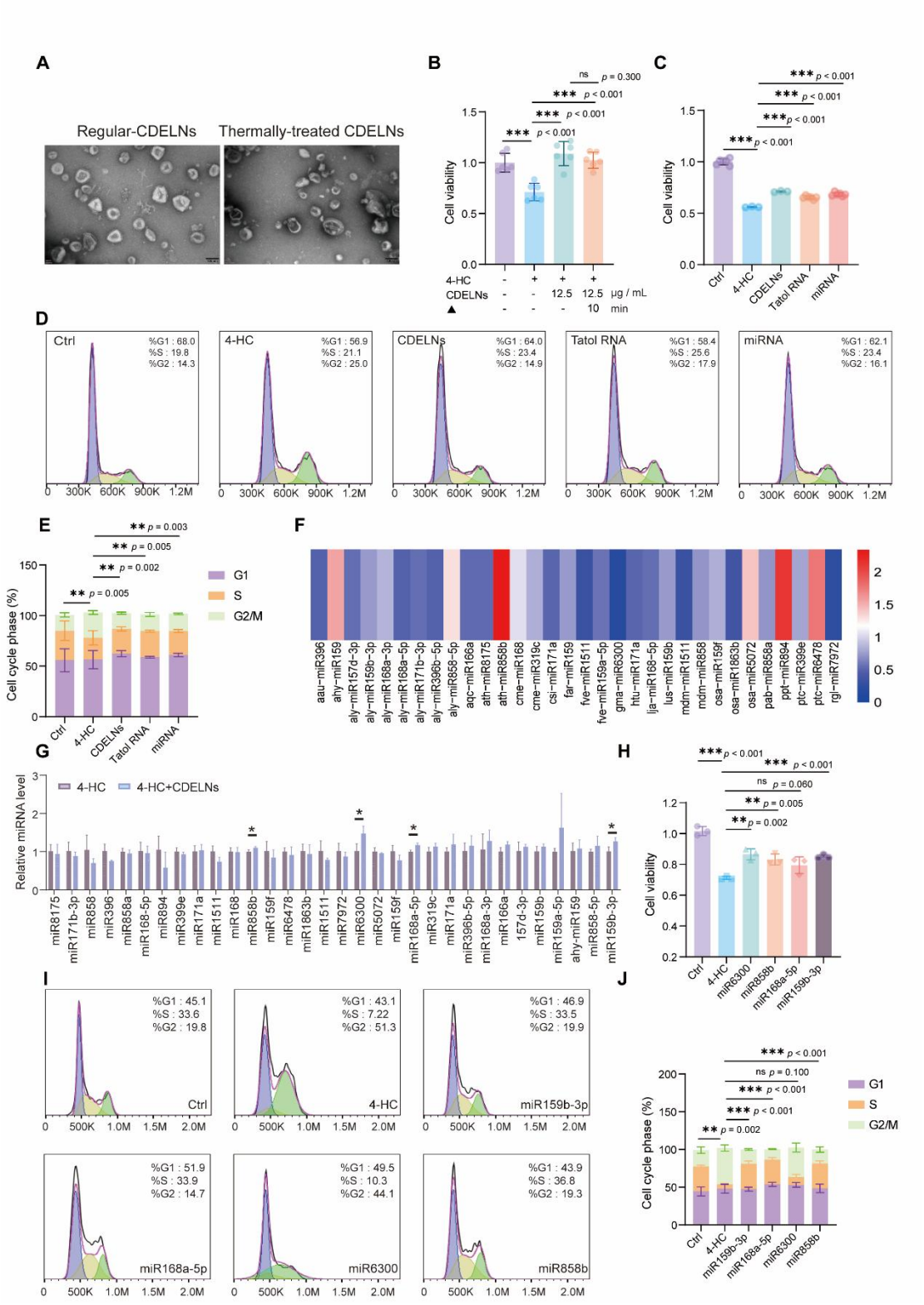

Fig. 4 | miRNAs derived from CDELNs exhibit protective effects on 4-HC induced injury in TM4 cells. A TEM images of CDELNs. Regular CDELNs: CDELNs were not be heated. Thermally-treated CDELNs: CDELNs were treated 98℃ for 10 min. **B** Heated CDELNs retained their ability to increase cell viability against 4-HC induced injury in TM4 cells ($n = 3$). **C** Total RNA

or miRNA from CDELNs increase cell viability against 4-HC induced injury in TM4 cells. **D** Total RNA or miRNA from CDELNs relieved 4-HC induced cell cycle arrest in TM4 cells by flow cytometric analysis. **E** Quantitative analysis of cell cycle phase in (**D**) (n = 3). **F** The expression levels of the 32 miRNAs from CDELNs with TPM > 1. **G** qRT-PCR analysis of miRNA expression in TM4 cells treated with CDELNs. **H** Three miRNAs (miR159b-3p, miR6300, miR858b) increased cell viability against 4-HC induced injury in TM4 cells. **I** Three miRNAs (miR159b-3p, miR168a-5p, miR858b) relieved 4-HC induced cell cycle arrest in TM4 cells by flow cytometric analysis. **J** Quantitative analysis of cell cycle phase in (**I**) (n = 3). All data are presented as the means ± SDs.

and miR858b significantly improved cell cycle arrest (Fig. 4H–J and Supplementary Fig. 4E–H). Collectively, these results indicate that these miRNAs are potential key bioactive components of CDELNs. They may bind to specific cell cycle-related genes and act as post-transcriptional regulators to downregulate the expression of target proteins by inhibiting translation or triggering mRNA degradation, thereby exerting reproductive protective effects.

CDELNs rescue 4-HC-induced Sertoli cell injury through miR159b-3p/P21

To investigate whether CDELNs derived miRNAs target P21, we transfected miR159b-3p, miR6300 and miR858b mimics in TM4 cells, respectively, and tested P21 expression level. qRT-PCR analysis showed that all three miRNAs significantly inhibited the 4-HC-induced upregulation of P21 expression; notably, miR159b-3p exhibited the most prominent inhibitory effect, reducing P21 expression by approximately 50% compared to the 4-HC treated group (Fig. 5A). Similar results were obtained via Western blot analysis (Fig. 5B, C). In addition, we verified the binding interaction between miR159b-3p and *P21* mRNA 3'UTR using a dual-luciferase reporter assay. miR159b-3p mimic significantly inhibited the relative luciferase activity of the wild-type (WT) *P21* 3'UTR, but had no significant effect on the mutant (MUT) 3'UTR in 293T cells (Fig. 5D, E). This indicates that miR159b-3p can post-transcriptionally regulate P21 expression by targeting mRNA 3'UTR.

To further explore the function of miR159b-3p, gain-of-function and loss-of-

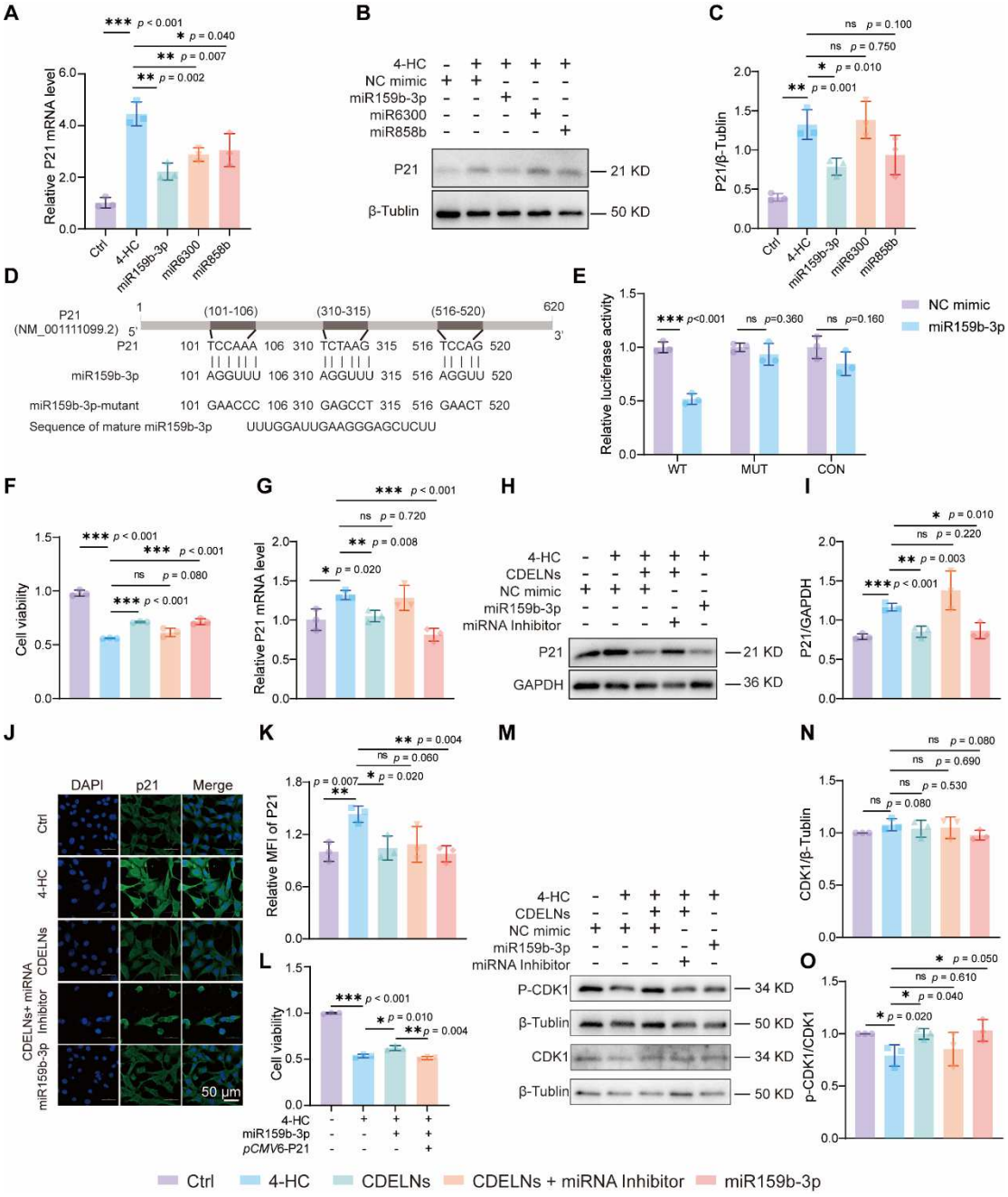

Fig. 5 | CDELNs ameliorate Sertoli cell injury via miR159b-3p/P21. A qRT-PCR analysis of P21 gene expression in TM4 cells treated with 4 μM 4-HC upon intervention with the three miRNAs (miR159b-3p, miR6300, and miR858b). **B** Western blot analysis of P21 protein expression in TM4 cells treated with 4 μM 4-HC upon intervention with the three miRNAs (miR159b-3p, miR6300, and miR858b). **C** Quantitative analysis of P21 expression in (**B**) ($n = 3$). **D** Putative binding sites of miR159b-3p at P21 mRNA 3'UTR. **E** Dual luciferase reporter assay to verify binding interaction between miR159b-3p and P21 mRNA 3'UTR in 293T cells co-transfected with either pmiR-GLO empty vector, pmiR-GLO-P21-3'UTR-WT, or pmiR-GLO-P21-3'UTR-MUT reporter plasmids,

along with miR159b-3p mimic or negative control (NC) mimic. **F** miR159b-3p mimic increased cell viability against 4-HC induced injury in TM4 cells. Inversely, miR159b-3p inhibitor attenuated the protective effects of CDELNs. **G** qRT-PCR analysis of P21 gene expression in TM4 cells treated with 4 μM 4-HC upon intervention with CDELNs, CDELNs+ miR159b-3p inhibitor, or miR159b-3p mimic (n = 3). **H** Western blot analysis of P21 gene expression in TM4 cells treated with 4 μM 4-HC upon intervention with CDELNs, CDELNs + miR159b-3p inhibitor, and miR159b-3p mimic. **I** Quantitative analysis of P21 expression in (**H**) (n = 3). **J** Representative immunostaining images of P21 in TM4 cells treated with 4 μM 4-HC under the interventions of CDELNs, CDELNs + inhibitor, and miR159b-3p mimic. **K** Quantitative analysis of mean fluorescence intensity of P21 in (**J**) (n = 3). **L** P21 overexpression reduced cell viability of TM4 cells treated with 4 μM 4-HC upon intervention with miR159b-3p (n = 3). **M** Western blot analysis of CDK1 and p-CDK1 in TM4 cells treated with 4 μM 4-HC under the interventions of CDELNs, CDELNs + inhibitor, and miR159b-3p mimic. **N, O** Quantitative analysis of CDK1 (**N**) and p-CDK1/CDK1 (**O**) expression in (**M**) (n = 3). All data are presented as the means ± SDs.

function research were conducted in TM4 cells. Overexpression of miR159b-3p effectively reversed the 4-HC-induced decrease in cell viability, mimicking the protective effect of CDELNs. Conversely, inhibiting miR159b-3p function with its inhibitor significantly attenuated the protective effect of CDELNs (Fig. 5F). This confirms that miR159b-3p is very critical for mediating the beneficial effects of CDELNs. At the molecular level, both qRT-PCR and Western blot analysis verified that overexpression of miR159b-3p significantly inhibited the 4-HC-induced upregulation of P21 mRNA and protein levels, while inhibition of miR159b-3p exerted the opposite effect (Fig. 5G–I). Similar results of P21 were observed via immunofluorescence imaging (Fig. 5J, K). More importantly, overexpression of P21 significantly attenuated the beneficial effect of miR159b-3p on cell viability (Fig. 5L), which further confirms that P21 is its key target. Collectively, miR159b-3p rescues 4-HC-induced Sertoli cell injury by directly targeting P21 and inducing its mRNA degradation.

CDK1 (also known as Cdc2) is a core kinase that drives the G2/M phase transition of the cell cycle, and its activity is negatively regulated by the CDK inhibitor P21[55,56].

Given that miR-159b-3p derived from CDELNs can target and inhibit P21 expression, we further investigated its regulatory role on CDK1 activity. Western blot analysis showed that 4-HC treatment did not alter CDK1 protein levels but significantly suppressed phosphorylation at its critical activation site, Thr161. Both CDELNs intervention and miR-159b-3p overexpression effectively rescued this suppression, restoring CDK1 phosphorylation to normal levels. In contrast, inhibition of miR-159b-3p abolished the ability of CDELNs to restore CDK1 activity (Fig. 5M-O). These findings indicate that miR-159b-3p delivered by CDELNs may alleviate 4-HC-induced G2/M phase arrest by targeting P21, thereby relieving its inhibition of the CDK1 and promoting CDK1 phosphorylation and activation.

Biodistribution of CDELNs and miRNA delivery *in vivo*

Prior to evaluating the efficacy of CDELNs in repairing testicular reproductive injury *in vivo*, we investigated the testicular accumulation of CDELNs in C57BL/6 mice. The CDELNs labeled with fluorescent dye DiR (DiR-CDELNs) were intraperitoneally administered to mice, and the DiR fluorescence signals from mice were tracked continuously using an *in vivo* imaging system. As indicated in Fig. 6A, DiR-CDELNs exhibited significant accumulation in mice compared to the DiR dye-only group within 48 h. At different time points, mice were sacrificed, and fluorescence intensity in serum and major organs was detected using fluorescence correlation spectroscopy (FCS). The fluorescence signal in serum peaked at 4 h after DiR-CDELNs injection and then steadily decreased, indicating that CDELNs effectively entered the circulatory system (Fig. 6B). Notably, DiR-CDELNs showed obvious accumulation in testicular tissue, with a steady increase in fluorescence signal over time (Fig. 6C). Additionally, persistent fluorescence signals were detected in the liver, spleen, and kidney within 48 h (Supplementary Fig. 5A). These findings demonstrate that the nanovesicle structure of CDELNs endows them with favorable *in vivo* circulation stability and a prolonged retention time, as well as the potential to accumulate in testicular tissue, laying a pharmacokinetic foundation for their reproductive protective effects. To verify the efficacy of CDELNs as a delivery vector for functional miRNA, in situ hybridization

was used to detect miR159b-3p in testicular tissue sections. Compared with the control group, the CDELNs-treated group exhibited a significant increase in the specific hybridization signal of miR159b-3p in testicular tissue (Fig. 6D, E). This indicates that CDELNs successfully deliver and release functional miRNA cargo into testicular tissue.

Biosafety of CDELNs *in vivo*

In accordance with drug safety evaluation guidelines, *in vitro* hemolysis assays are necessary for injectable formulations that may enter the systemic circulation to rule out the risk of hematotoxicity[57]. CDELNs were co-incubated with freshly isolated murine erythrocytes at 37 °C for 3 h across a concentration gradient of 25–100 μg/mL, using Triton X-100 and PBS as positive and negative controls, respectively. Hemolytic analysis demonstrated that all CDELNs-treated specimens maintained optical clarity without visible hemolysis or precipitate formation, showing no significant difference from the negative control. Absorbance measurements further confirmed CDELNs did not induce RBC rupture or hemoglobin release across the tested concentrations, and thus exhibited no significant hemolytic activity (Fig. 6F, G). To further evaluate systemic biosafety of CDELNs *in vivo*, healthy C57BL/6J mice were selected for CDELNs administration intraperitoneally at a dose of 2.5 mg/kg/d for two weeks, with gender-, age-, and weight-matched mice treated with PBS serving as controls. In the biosafety evaluation system for nanomedicines, monitoring the effect of drugs on mouse body weight provides an initial assessment of potential systemic toxicity[58]. During the two-week administration period, no significant difference was observed in the body weight growth curves between the CDELNs-treated group and the control group, indicating that CDELNs did not cause systemic adverse effects (Supplementary Fig. 5B). After two weeks of administration, serum biochemical, hematological, and histological analyses were performed. Serological tests showed no significant changes in key indicators related to liver and kidney function, including alanine transaminase (ALT), aspartate transaminase (AST), albumin (ALB), and uric acid (UA) (Fig. 6H). Hematological parameters such as neutrophil (Neu), white blood cell (WBC), lymphocyte (Lym), and red blood cell (RBC) counts were all within physiological

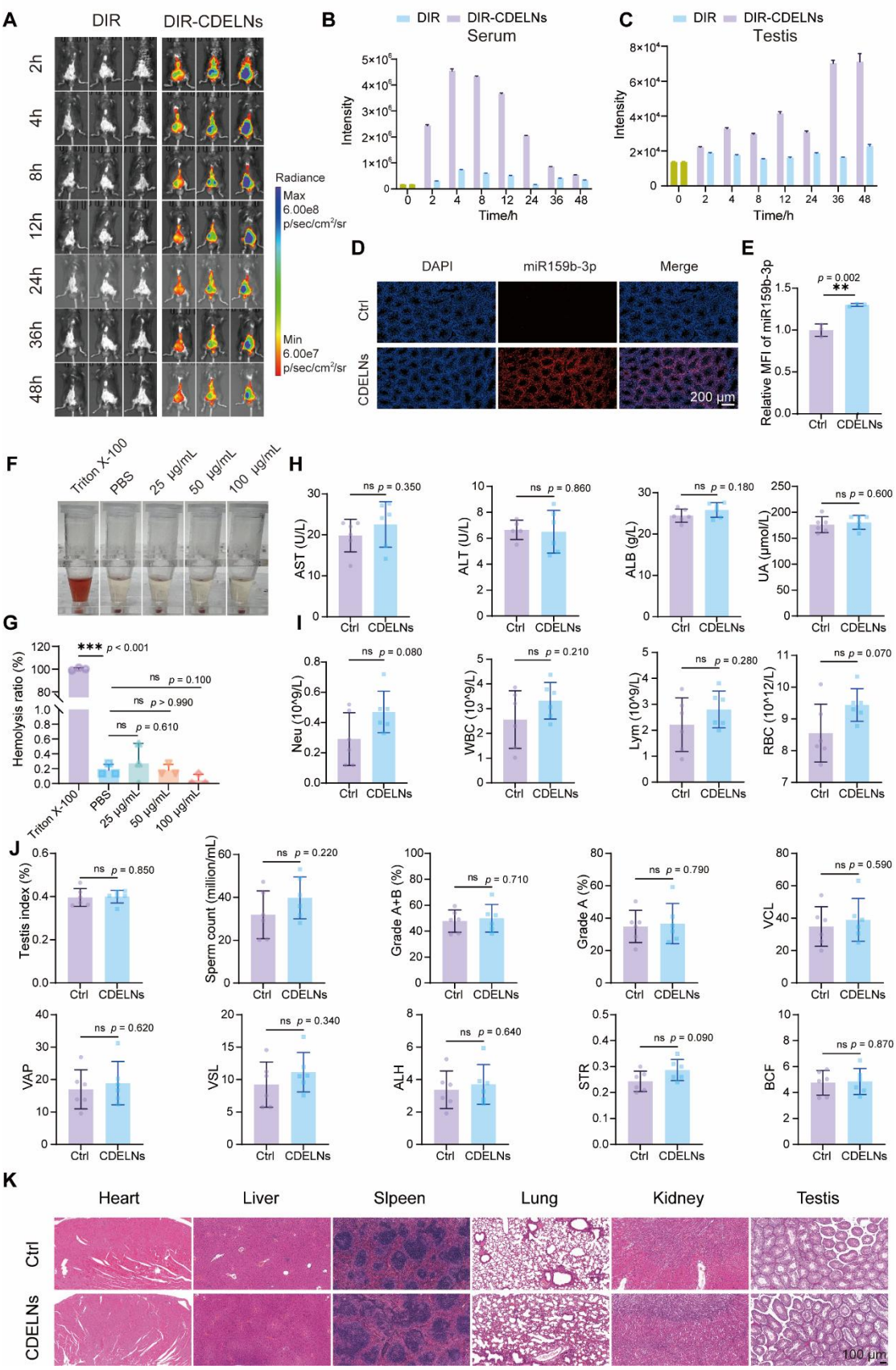

Fig. 6 | *In vivo* biodistribution and biosafety evaluation of CDELNs. A Small animal *in vivo* imaging at 2, 4, 8, 12, 24, 36, and 48 h after intraperitoneal injection of DiR or DiR-CDELNs. **B, C**

Fluorescence intensity of DiR or DiR-CDELNs in mouse serum and testis. Data are presented as the means ± SEMs. *n* = 10 technical replicates. **D** miRNA in situ hybridization in testicular sections from mice treated with PBS or CDELNs. **E** Quantitative analysis of mean fluorescence intensity of miRNA in (**D**) (*n* = 3). **F** Hemolysis assay of erythrocytes incubated with 0.1% Triton X-100, PBS and different concentrations (25, 50, 100 μg/mL) of CDELNs. **G** Quantitative analysis of hemolysis ratio through absorbance measurement in (**F**) (*n* = 3). **H** Serum levels of AST, ALT, ALB, and UA in mice after 14 days of intraperitoneal CDELNs injection (*n* = 6). **I** Levels of Neu, WBC, Lym, and RBC in diluted blood from mice after 14 days of intraperitoneal CDELNs injection (*n* = 6). **J** Testicular index, sperm concentration and sperm motility in mice after 14 days of intraperitoneal CDELNs injection (*n* = 6). **K** Representative H&E-staining images from heart, liver, spleen, lungs, kidneys, and testes of mice after 14 days of intraperitoneal CDELNs injection (*n* = 6). Data are presented as the means ± SDs.

ranges (Fig. 6I and Supplementary Fig. 5C), suggesting that CDELNs did not induce hematopoietic system disorders. Notably, evaluation of the male reproductive system revealed no significant adverse effects of CDELNs on testicular index using the ratio of testis to body weight, and sperm concentration and sperm motility as assessed by computer assisted sperm analysis (CASA) (Fig. 6J). In addition, histological evaluations of five major organs (heart, liver, spleen, lung, kidney) and testis via hematoxylin and eosin (H&E) staining showed that CDELNs did not cause obvious morphological abnormalities or tissue damage (Fig. 6K). These findings demonstrate that CDELNs exhibit no observable *in vivo* toxic effects at the administered dose and possess a favorable preliminary biosafety profile.

CDELNs ameliorate cyclophosphamide-induced testicular injury in mice by regulating the cell cycle pathway

In vitro experiments demonstrated that CDELNs treatment ameliorates 4-HC-induced decreases in TM4 cell viability and cell cycle arrest via the miR159b-3p/P21 axis. Encouraged by these promising results, we investigated the therapeutic potential and underlying mechanism of CDELNs on cyclophosphamide (CP)-induced testicular

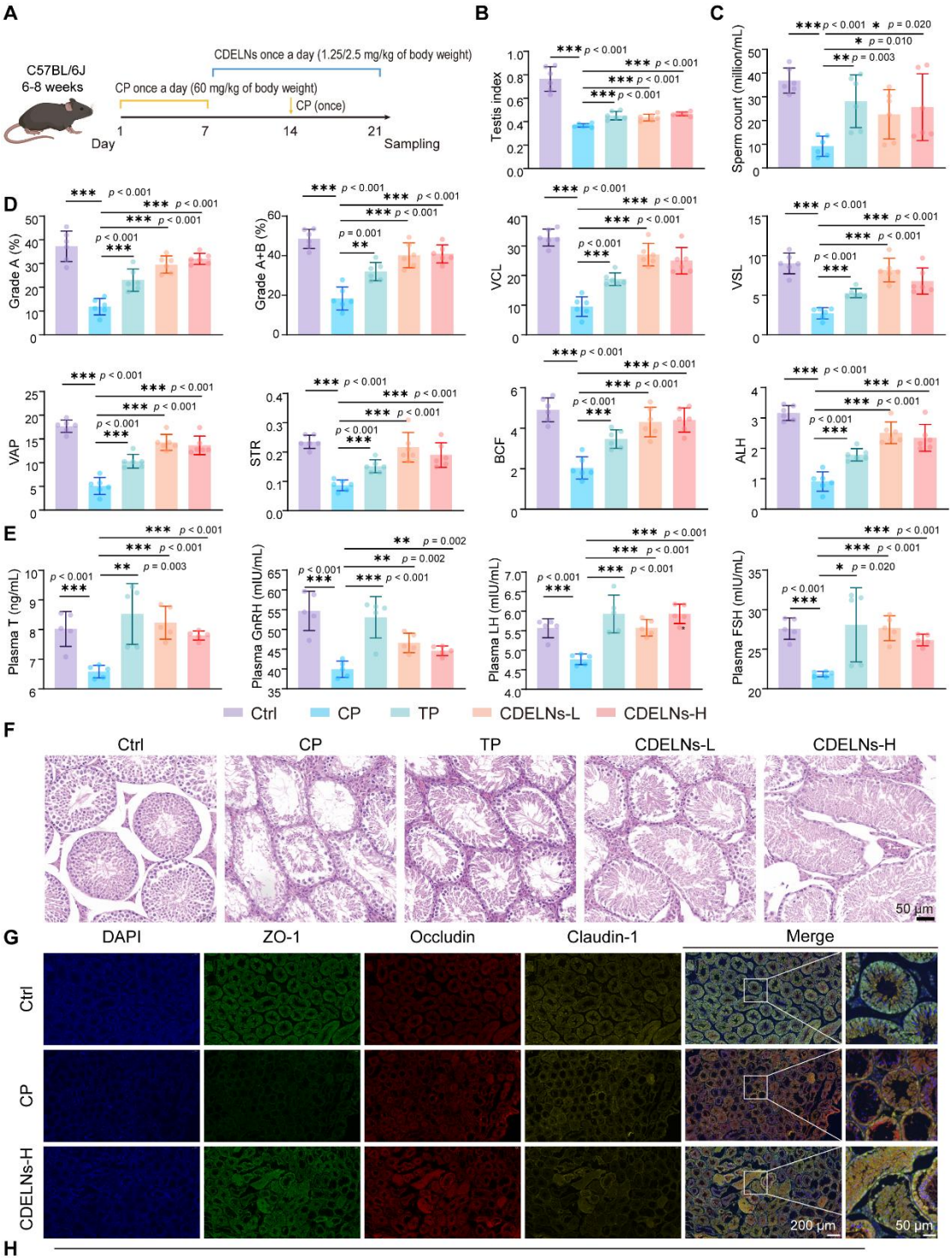

H

	Ctrl	CP	TP	CDELNs-L	CDELNs-H
Conception Rate	41.7%	0	0	16.7%	16.7%
Litter Size	43	0	0	2	3
Survival Rate at Birth	41/43	0	0	1/2	3/3

Fig. 7 | CDELNs ameliorate CP-induced male reproductive injury. A Schematic of the experiment *in vivo*. **B** Testicular index in CP-treated mice under the interventions of CDELNs and TP (n = 6). **C, D** CASA analysis of sperm concentration (**C**) and motility (**D**) in CP-treated mice

under the interventions of CDELNs and TP. Grade A: Sperms with rapid progressive motility, Grade A+B: Sperms with rapid and slow progressive motility. VCL: Curvilinear velocity. VSL: Straight-line velocity. VAP: Average path velocity. STR: Straightness. BCF: Beat-cross frequency. ALH: Amplitude of lateral head displacement (n = 6). **E** Serum levels of T, GnRH, LH and FSH in CP-treated mice under the interventions of CDELNs and TP (n = 5). **F** Representative H&E-staining images of testicular sections from CP-treated mice under the interventions of CDELNs and TP (n = 3). **G** Representative immunostaining images of ZO-1, Occludin, and Claudin-1 in testicular sections from CP-treated mice under the interventions of CDELNs (n = 3). H Fertility assessment of male mice treated with CP upon CDELNs and TP interventions (n (male mice) = 6, n (female mice) =12). All data are presented as the means ± SDs.

injury in mice. Specifically, after 7 consecutive days of cyclophosphamide injection, mice received daily treatments with PBS (control), CDELNs (high dose (H), 2.5 mg/kg; low dose (L), 1.25 mg/kg), or the positive control drug testosterone propionate (TP, 0.20 mg/kg, twice weekly) for 2 weeks. During this treatment period, CP was supplemented once every 7 days, and the experiment was terminated on day 14 of CDELNs administration (Fig. 7A). CP treatment significantly reduced mouse body weight and testicular index compared to the control group, which were partially restored following CDELNs administration (Fig. 7B and Supplementary Fig. 6A). CASA analysis of mouse sperm showed that CDELNs significantly improved sperm concentration and motility. Notably, in terms of sperm motility and progressive motility, the efficacy of CDELNs even exceeded that of the positive control TP (Fig. 7C, D). Additionally, enzyme-linked immunosorbent assay (ELISA) was used to detect key male endocrine hormones in serum, including testosterone (T), gonadotropin-releasing hormone (GnRH), luteinizing hormone (LH) and follicle-stimulating hormone (FSH). CP treatment decreased the levels of these hormones, while CDELNs reversed this reduction, confirming that CDELNs improve testicular endocrine function (Fig. 7E). Histopathological analysis revealed that CP induced a reduction in seminiferous tubule diameter, and epithelial thickness, which was accompanied by a loss of spermatocytes and a loosening of the cellular arrangement. CDELNs effectively and significantly

alleviated these injuries (Fig. 7F). Given the protective effect of CDELNs on Sertoli cells *in vitro*, we further investigated whether CDELNs could improve the blood-testis barrier (BTB) integrity *in vivo*, which is established and maintained by Sertoli cells[59,60]. Occludin, Claudin, and ZO-1 are the core proteins that constitute cellular tight junctions, serving as the structural foundation for maintaining barrier functions (such as the blood-testis barrier and blood-brain barrier)[61–63]. Immunofluorescence analysis of tight junction proteins showed that CP treatment reduced the fluorescence intensity of these proteins, particularly ZO-1, along with a decrease in their co-localization regions, which were significantly reversed by CDELNs (Fig. 7G). These findings suggest that CDELNs can alleviate Sertoli cell injury and enhance their function *in vivo*. Finally, we evaluated the effects of CDELNs on male fertility. The results showed that CP completely abolished the fertility of male mice, while CDELNs treatment significantly increased the mating success rate and offspring number (Fig. 7H). These findings demonstrate that CDELNs can alleviate testicular reproductive injury in mice.

To further verify the molecular mechanism underlying the protective role of CDELNs against testicular injury *in vivo*, we performed transcriptomic sequencing on testicular tissues. KEGG pathway enrichment analysis of differentially expressed genes revealed a significant enrichment in the cell cycle pathway (Fig. 8A, B), which was highly consistent with the results of *in vitro* cell experiments. In addition, Gene Set Enrichment Analysis (GSEA) to explore specific signaling pathways involved in the cell cycle showed that the p53 signaling pathway was specifically activated, which is consistent with its well-established role under cellular stress[64,65]. In contrast, the FoxO and mTOR signaling pathways showed no significant changes (Supplementary Fig. 7A – C). This suggests that the p53 pathway plays a critical role in this process, potentially inducing cell cycle arrest under CP stimulation by regulating the transcription of its downstream target gene P21. To validate this, we examined the expression of the key regulatory factor P21 in testicular tissues. Western blot, qRT-PCR, and immunofluorescence consistently confirmed that CDELNs treatment significantly reversed the CP-induced overexpression of P21 (Fig. 8C–G). Subsequently, we detected CDK1, the key downstream protein of P21, and found that CDELNs also reversed the

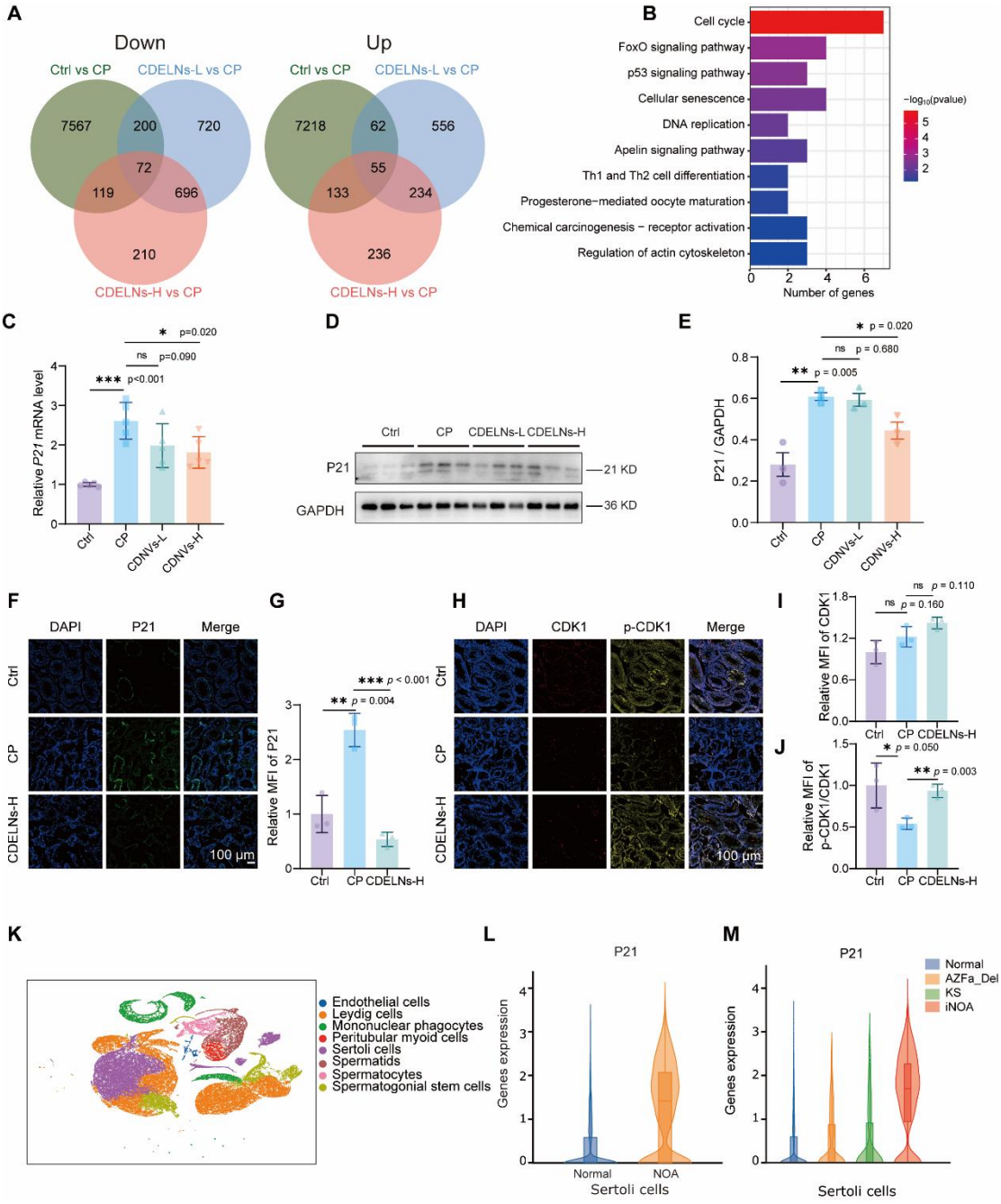

Fig. 8 | CDELNs ameliorate CP-induced male reproductive injury through relieving cell cycle arrest. A Venn diagrams of the mouse testicular transcriptomics data. **B** KEGG pathway enrichment analysis of differently expressed genes that were consistently regulated by CP, CDELNs-L, and CDELNs-H. **C** qRT-PCR analysis of P21 gene expression in CP-treated mice testes under the interventions of CDELNs (n = 5). **D** Western blot analysis of P21 protein expression in CP-treated mice testes under the interventions of CDELNs. **E** Quantitative analysis of P21 protein expression in (**D**) (n = 3). **F** Representative immunostaining images of P21 in testicular sections from CP-treated mice under the interventions of CDELNs. **G** Quantitative analysis of mean fluorescence

intensity of P21 in (**F**) (*n* = 3). **H** Representative immunostaining images of CDK1 and p-CDK1 in testicular sections from CP-treated mice under the interventions of CDELNs. **I, J** Quantitative analysis of mean fluorescence intensity of CDK1 (**I**) and p-CDK1/CDK1 (**J**) in (**H**) (*n* = 3). **K** UMAP plots of all testicular cells from single-cell transcriptome profiling of normal controls and NOA patients in public database. **L** Violin plot of the expression levels of P21 in normal and NOA Sertoli cells (*n* (Normal) = 6, *n* (NOA) = 7). **M** Violin plot of the expression levels of P21 in normal and three types of pathological NOA Sertoli cells **(***n* (Normal) = 6, *n* (AZFa_Del) = 1, *n* (KS) = 3, *n* (iNOA) = 3). All data are presented as the means ± SDs.

CP-induced reduction in the activating phosphorylation level of CDK1 (Fig. 8H–J). These results validate the molecular mechanism of CDELNs in rescuing testicular injury via the P21/CDK1-mediated cell cycle pathway.

Non-obstructive azoospermia (NOA) is the most severe form of male factor infertility, affecting 10%–15% of infertile men[66,67]. It is commonly classified into three subtypes, Klinefelter syndrome (KS, with an extra X chromosome), Y chromosome AZFa region microdeletion (AZFa_Del), and idiopathic NOA (iNOA) of unknown causes[68–70]. Among these, iNOA accounts for 80% of cases, which is clinically intractable and lacks effective treatments[71,72]. To evaluate the clinical translation potential of CDELNs, we conducted an in-depth analysis of publicly available single-cell transcriptome dataset from LiangYu Zhao and colleagues[73]. The results showed that compared with healthy individuals (Normal), Sertoli cell populations in the testicular tissues of NOA patients exhibited significant transcriptomic differences, with the most prominent deviation observed in iNOA patients (Fig. 8K and Supplementary Fig. 7D). This suggests that Sertoli cells may play a central role in the pathological progression of NOA, which is consistent with previous reports. Notably, our in-depth analysis revealed that the P21 gene was universally upregulated in the testicular tissues of NOA patients, with specific high expression in Sertoli cells (Fig. 8L and Supplementary Fig. 7E). This indicates that despite the varied initial etiologies of NOA, P21 activation may be one of the common downstream pathogenic pathways. Further analysis of different NOA subtypes confirmed that P21 was consistently upregulated in patients with KS,

AZFa_Del, and iNOA; among these, the most significant upregulation was observed in iNOA patients (Fig. 8M). Collectively, these bioinformatics analyses reveal that Sertoli cells and the regulatory factor P21 are critically involved in male reproductive disorders. This bridges the P21-targeting mechanism of CDELNs with the most urgent clinical treatment needs, suggesting that P21-targeted intervention strategies, particularly CDELNs-based therapies, hold great promise for providing a novel therapeutic approach to clinically refractory iNOA.

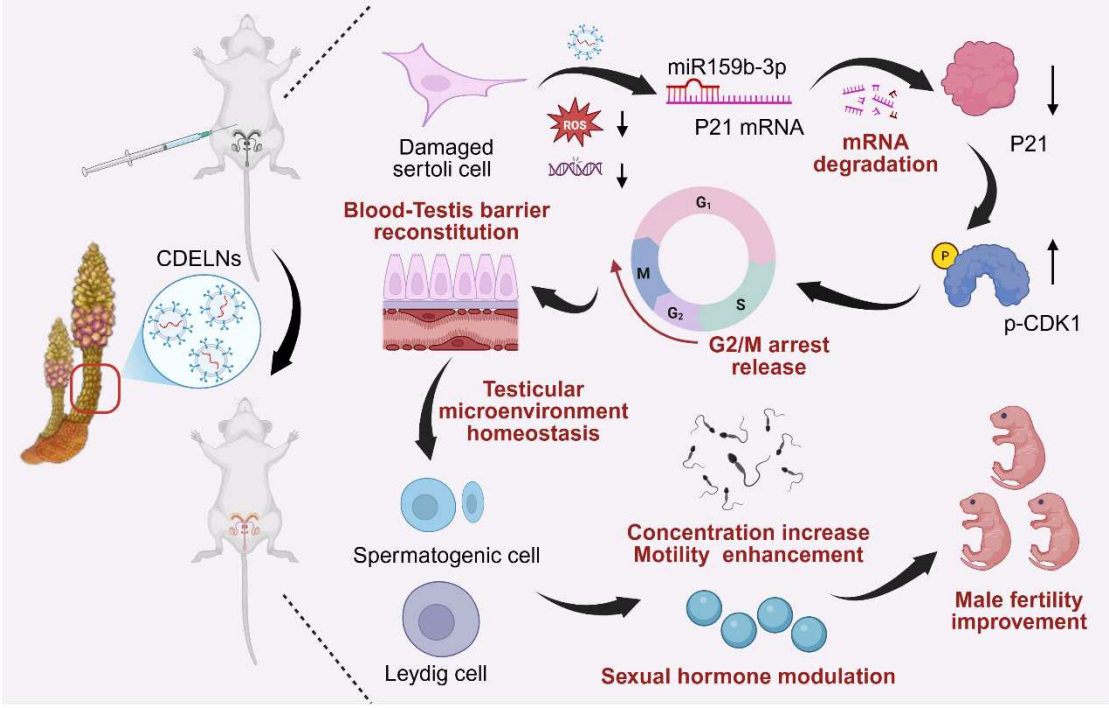

Fig. 9 | Schematic illustration of CDELNs ameliorate cyclophosphamide-induced testicular injury. miR159b-3p derived from CDELNs binds to the 3'UTR of P21 mRNA to suppress its expression, which enhances CDK1 phosphorylation, alleviates cyclophosphamide-induced cell cycle arrest, and boosts Sertoli cell proliferation. This process improves the blood-testis barrier in mouse testes, maintains testicular microenvironment homeostasis, consequently reinstates the production of the sex hormone testosterone, improves sperm concentration and motility, and ultimately enhances male fertility.

Discussion

Male infertility accounts for about 50% of infertility cases, primarily manifested as sperm quality abnormalities including oligozoospermia, asthenozoospermia, and azoospermia[74,75]. Among various causative agents, chemotherapeutic drugs arise a significant concern[76]. Cyclophosphamide (CP), one of the most commonly used chemotherapeutic agents, has been extensively demonstrated to severely impair male reproductive function[77]. Clinical studies have shown that CP-treated male cancer patients exhibit varying degrees of reduced sperm count and motility. Notably, approximately 90% of male children treated with CP develop azoospermia or oligozoospermia in adulthood[78,79]. These findings underscore the urgent need to elucidate the mechanisms of CTX-induced reproductive damage and develop effective interventions.

Current clinical interventions for male reproductive injury lack specific therapies, relying primarily on non-specific protection or symptomatic support. For instance, antioxidants (e.g., melatonin, vitamin E) are used to mitigate oxidative stress-induced damage, and hormones (e.g., testosterone propionate) are administered to maintain reproductive endocrine balance[80,81]. Despite their clinical applications, these approaches generally suffer from unclear mechanisms, limited therapeutic efficacy, and potential safety risks with long-term use. Certain plant-derived extracts exhibit reproductive protective effects, yet their complex components and targets hinder the precise therapeutic intervention. Emerging strategies, such as stem cell transplantation (e.g., mesenchymal stem cells, spermatogonial stem cells) has shown promise in repairing testicular injury and promoting spermatogenesis in animal models through paracrine effects or direct differentiation[82,83]. However, its clinical application is still constrained by risks of teratoma formation and immune rejection. Similarly, while nanomaterials (e.g., selenium nanoparticles, cerium dioxide nanoparticles) can mimic superoxide dismutase (SOD) activity to reduce reactive oxygen species (ROS)-induced sperm damage, their potential biocompatibility issues and long-term *in vivo* toxicity remain limit the clinical translation[84,85].

Plant-derived exosome-like nanovesicles (PELNs), which share structural and compositional similarity with mammalian exosomes, serve as effective vehicles for cross-kingdom regulation[86,87]. Their cargo of plant-derived miRNAs can be delivered across species to exert functional gene regulatory effects in recipient organisms[88,89]. In recent years, PELNs have demonstrated significant therapeutic potential in various disease models. For example, exosome-like nanovesicles derived from *Brucea javanica* fruits deliver 10 specific miRNAs to regulate the PI3K/Akt/mTOR signaling pathway and activate ROS/Caspase-mediated apoptosis, thereby suppressing triple-negative breast cancer progression[90]. Ginger-derived exosome-like nanovesicles deliver mdo-miR7267-3p to target gut microbiota, inhibiting monooxygenase ycnE in *Lactobacillus rhamnosus*, which reshapes the gut immune microenvironment and enhance the mucosal barrier function, and ultimately alleviate colitis[89]. Despite the significant therapeutic potential of PELNs in anti-inflammation, anti-tumor, and immunomodulation, their role in male reproductive protection has not been explored to date. Here, our study firstly demonstrates that CDELNs can effectively reverse CP-induced reproductive injury by delivering miR159b-3p to testicular tissue, achieving a breakthrough application of PELNs in male reproductive protection and opening new avenues for cross-kingdom regulatory research.

The traditional Chinese medicine *C. deserticola* is widely used in clinical prescriptions for male infertility due to its kidney-tonifying and essence-replenishing properties. Its traditional efficacy is mostly attributed to small-molecule compounds (e.g., phenylethanoid glycosides) rather than exosome-like nanovesicle[89]. While pharmacological studies have initially confirmed the reproductive protective effects of phenylethanoid glycosides, their clinical translation and modern formulation development are hampered by low bioavailability and unclear mechanisms[91,92]. This study shifts the paradigm by identifying and validating CDELNs as a novel, efficacious nanomaterial for treating male reproductive injury. As a newly discovered bioactive component of *C. deserticola*, CDELNs have the potential to overcome the limitations of traditional extracts and open new avenues for developing *Cistanche*-based pharmaceuticals and health products.

CDELNs exhibit unique advantages over existing therapeutic approaches for male reproductive diseases. First, as naturally derived nanovesicles, CDELNs possess excellent biocompatibility and stability, supported by no observed side effects in mice at the tested doses, which overcoming the safety risks of chemical drugs, stem cell therapies, and synthetic nanoparticles. Second, CDELNs have great testis-targeting ability because their nanoscale size enables efficient penetration of the blood-testis barrier (BTB) and enhanced accumulation in testicular tissue. Finally, they are natural nanosystems with well-defined active components, delivering encapsulated functional miRNAs to testicular tissue to ameliorate injury via precise mechanisms, such as P21-targeted cell cycle regulation. Thus, CDELNs uniquely integrate the safety of natural products with the precision of targeted therapeutics, positioning them as a highly promising candidate for treating male reproductive injury.

Sertoli cells, the core structural cells of the testicular seminiferous epithelium, provide precise microenvironmental homeostasis for germ cells through physical support, nutrient supply, and immune privilege regulation, serving as a key regulatory hub for spermatogenesis[93]. The preferential uptake of CDELNs by Sertoli cells may initially improve their nutrient supply and structural support functions, thereby indirectly promoting the survival and proliferation of germ cells. This offers a novel perspective for understanding the role of testicular somatic cell in reproductive disorders. Moreover, *in vitro* experiments confirmed that CDELNs also directly alleviate the CP-induced cytotoxicity on testicular germ cells (GC1, GC2) and Leydig cells (TM3), demonstrating a broad cytoprotective effect across distinct testicular cell types (Supplementary Fig. 8). Concurrently, CDELNs exhibit pro-proliferative activity across these cell types (Supplementary Fig. 2A). These findings indicate CDELNs may counteract the reproductive toxicity of cyclophosphamide through multi-target and multi-pathway regulatory mechanisms, which provides an innovative protective strategy for chemotherapy-induced infertility.

The chemotherapeutic agent cyclophosphamide commonly induces DNA damage to activate the p53 pathway, which in turn triggers the abnormal overexpression of P21, a key cell cycle regulator, ultimately leading to cell cycle arrest[94–96]. However, specific

role of P21 in reproductive injury remains unclear. Our study reveals a novel therapeutic mechanism of CDELNs in counteracting CP-induced male reproductive injury. CDELNs deliver miR159b-3p, which precisely targets the 3' untranslated region (3'UTR) of P21 mRNA, significantly inhibiting its post-transcriptional expression. This downregulation relieves the inhibitory effect of P21 on CDK1, thereby reversing the cell cycle arrest of Sertoli cells, restoring their proliferation and blood-testis barrier function, and ultimately maintaining testicular spermatogenesis. Consequently, the sperm quality and fertility of CP-injured model mice are significantly improved. Furthermore, single-cell transcriptomic analysis of clinical patients confirmed a strong association between P21 dysregulation and male infertility. Thus, our study innovatively links P21 post-transcriptional regulation to male reproductive injury, establishing the P21 as a critical target and providing a new therapeutic framework for reproductive diseases.

Notably, the beneficial effects of CDELNs may not rely solely on miRNA regulation. As a naturally derived nanocarrier, CDELNs are also rich in bioactive metabolites (e.g., diglycerides, *N*-acylethanolamines), which can directly regulate metabolic pathways. More importantly, testicular metabolomic analysis showed that CDELNs intervention significantly reshapes the metabolic profile of CP-injured testes (Supplementary Fig. 9), suggesting that CDELNs may orchestrate a metabolic reprogramming of the testicular niche by regulating energy metabolism, amino acid metabolism, and lipid homeostasis, thereby providing metabolic support for the function recovery of germ cells.

In the process of drug development and clinical translation, safety evaluation of CDELNs is crucial. In this study, during CDELNs treatment (2.5 mg/kg, once daily for 14 days), no malformations were observed in animals, and normal body weight gain and food intake were maintained. Comprehensive assessment of male reproductive system showed that testicular organ coefficient and sperm count, motility and morphology were within the normal physiological range, indicating no significant reproductive toxicity of CDELNs. Furthermore, hematological and serum biochemical analyses, including liver and kidney function markers such as ALT, AST, ALB and UA,

revealed no biologically significant abnormalities, demonstrating that CDELNs did not cause obvious liver or kidney damage. Histopathological examination of the heart, liver, spleen, lungs, kidneys, and testes showed no pathological changes or drug-related toxic injury signs. Collectively, these results provide important evidence for the preliminary safety of CDELNs, while formal good laboratory practice (GLP) toxicological studies are required before clinical trials.

In conclusion, our findings demonstrate CDELNs effectively mitigate chemotherapy-induced testicular injury by delivering their miRNA that target P21, thereby alleviating Sertoli cell cycle arrest and restoring blood-testis barrier integrity. This process establishes a favorable microenvironment for germ cells and leydig cells, ultimately improving male fertility (Fig. 9). This work reveals a specific molecular target and a novel therapeutic strategy for reproductive injury, positioning CDELNs as a promising clinical therapeutic agent for the treatment of male infertility.

Methods

Ethics statement

All animal experiments adhered to the ethical regulations of Peking University, as approved by the Institutional Animal Care and Use Committee (DLASBE0645).

Animals

C57BL/6J mice (male, 6–8-week-old) were purchased from the Department of Experimental Animal of Peking University Health Science Center. All mice were housed under standardized conditions. The reproductive injury model of mice was established via daily intraperitoneal administration of cyclophosphamide (BD122998, Bide Pharmatech, China) (CP) (60 mg/kg) to C57BL/6J males over 7 consecutive days. Thereafter, the mice received daily treatments with PBS (control), CDELNs (high dose (H), 2.5 mg/kg; low dose (L), 1.25 mg/kg), or the positive control drug testosterone propionate (TP, 0.20 mg/kg, twice weekly) for 2 weeks. During this treatment period, CP was supplemented once every 7 days, and the experiment was terminated on day 14 of CDELNs administration. During the experiment period, the body weight of mice was

775 measured daily. When the experiment was terminated, blood samples were collected,
776 and bilateral testes were weighed and preserved for further analysis. The left
777 epididymals were excised for sperm quality assessment.

778 **Cell culture**

779 HEK293T cells, GC1, GC2, TM3 and TM4 cells were obtained from Cell Resource
780 Center (CRC) National BioMedical Cell-line Resource (BMCR). Cells were cultured
781 in dulbecco's modified eagle medium (Gibco, C11995500BT) with 10% fetal bovine
782 serum (Abcam, AB-FBS0500) and 1% penicillin-streptomycin solution (Macgene,
783 CC004). Culture procedures were carried out in a humidified Thermo incubator, set to
784 37°C and supplemented with 5% CO_2.

785 **Isolation, purification, and characterization of CDELNs**

786 CDELNs were extracted from *C. deserticola* juice using differential centrifugation. To
787 summarize, fresh *C. deserticola* was cleaned, chopped, and homogenized at a low
788 temperature to prepare the crude extract. The *C. deserticola* crude extract was then
789 centrifuged three times (1000 g for 10 min, 3000 g for 20 min, and 10,000 g for 30 min).
790 The supernatant was centrifuged at 100,000 g for 30 min. The resultant pellet was
791 resuspended in 2 mL of phosphate buffer (PBS) (G4202-500ML, servicebio, China)
792 and then loaded onto a pre-formed sucrose density gradient (30, 45, and 60%). After
793 ultracentrifugation at 150,000 g for 120 min, the intermediate bands were collected,
794 diluted with PBS, and subjected to another round of ultracentrifugation at 150,000 g for
795 60 min. The final material was resuspended in sterile PBS. The diameter and
796 concentration of the purified CDELNs were determined via Nanoparticle Tracking
797 Analysis (NTA) (Nanosight NS300, Malvern, Worcestershire, UK). Subsequent
798 analysis of zeta potential and polydispersity index (PDI) was conducted using a
799 Zetasizer (Zetasizer 3000, Malvern, Worcestershire, UK). Transmission electron
800 microscopy (TEM) (JEM-2100F, Hitachi, Kyoto, Japan) was used to analyze the
801 morphology of the CDELNs.

802 **Quantification of CDELNs**

803 20 μL of the resuspended sample was aliquoted in triplicate into a 96-well plate, and
804 the BCA kit (DQ111-01, TransGen, China) was employed as described in the

manufacturer's instructions. Absorbance measurement at 562 nm, following incubation with the BCA working solution at 37 ℃ for 30 min, enabled the calculation of CDELN concentration using a standard curve.

Lipidomic Analysis

Lipidomic profiling was conducted using an Ultimate 3000 UHPLC system coupled to a Q-Exactive HF MS (Thermo Fisher Scientific, Waltham, MA, USA). Chromatographic separation was achieved on a reversed-phase BEH C18 column (2.1 mm × 100 mm, 2.5 μm, Waters, USA) maintained at a constant temperature of 40 °C. The software employs its integrated LipidBlast in silico spectral database (version: LipidDBs-VS23-FiehnO) to provide the MS/MS data required for extracting chromatographic peaks and quantifying lipid species.

Metabolomic Analysis

Metabolomics analysis was performed on an Ultimate 3000 UHPLC system coupled with Q-Exactive HF MS (Thermo Fisher Scientific, Waltham, MA, USA). For metabolomics, an XBridge amide column (100 × 2.1 mm i.d., 3.5 μm; Waters, USA) was used at 30 °C. Compound identification was performed according to a previously published procedure[97].

Proteomic Analysis

The protein extract from lysed CDELNs was denatured and resolved on a 10% SDS-PAGE gel. Excised gel bands were subjected to in-gel digestion with trypsin. The resulting peptides were analyzed by LC-MS/MS on a Thermo Vanquish Neo system coupled to a Thermo Orbitrap Astral mass spectrometer. Separation was performed on a PepMap RSLC C18 column (150 μm ID, 150 mm length). Mass spectrometry data were acquired in data-independent acquisition mode controlled by Xcalibur 4.7 software, comprising a full-scan Orbitrap spectrum (*m*/*z* 380–980, 240,000 resolution) followed by data-independent MS/MS scans. All MS/MS spectra were processed using Proteome Discovery (version 3.1) for database search and protein identification.

RNA sequencing

Total RNA was isolated with TRIzol reagent (15596018CN, Invitrogen, USA), and its

integrity was evaluated through agarose gel electrophoresis along with an Agilent 2100 Bioanalyzer (Agilent Technologies, USA). Subsequently, cDNA libraries were prepared and subjected to sequencing using an Illumina HiSeq2500 platform at BGI Genomics (China). To identify differentially expressed genes across comparison groups, the DESeq2 software was applied, utilizing a significance threshold of p-value < 0.05 and a |fold change| $\geqslant$ 1.5.

miRNA Sequencing

miRNA sequencing was performed by BGI Genomics. The total isolated RNA underwent purification was sequentially ligated with 3' and 5' adapters through incubation steps. Reverse transcription was performed using a prepared reaction mixture in a programmed thermocycler, followed by PCR amplification. The resulting PCR products were purified by PAGE gel electrophoresis and recovered in EB solution. Depending on product requirements, an appropriate quality control protocol was selected. Single-stranded PCR products were denatured and then circularized using a specifically configured reaction system. Following enzymatic digestion of uncyclized linear DNA, the resulting single-stranded circular molecules were utilized as templates for rolling circle amplification, yielding DNA nanoballs (DNBs) comprising multiple copies. Quality-qualified DNBs were then assembled onto patterned nanoarrays using high-intensity DNA nanochip technology and subjected to sequencing through combinatorial Probe-Anchor Synthesis (cPAS).

Stability of CDELNs *in vitro*

CDELNs were treated with simulated bodily fluid (MX0952, maokangbio, China) (SBF) and phosphate-buffered saline (PBS) for 0, 1, 3, 6, 12, 24, and 48 h. The changes in particle size were analyzed using nanoparticle tracking analysis.

Cellular uptake of CDELNs

GC1, GC2, TM3, and TM4 cells were maintained at 37 °C in 5% CO_2 for 16h. DiD (ab275319, Abcam, UK)-labeled CDELNs (25 μg/mL) were co-incubated with these cells for 24 h in the IncuCyte S3 Live-Cell Analysis System (Sartorius, Germany) for continuously monitoring total cells and DiD positive cells. To analyze the uptake

kinetics, TM4 cells were co-incubated with DiD-labeled CDELNs for different durations (3, 6, 12, and 24 h) and then were collected for flow cytometry analysis (CytoFLEX, Beckman Coulter, Inc., USA). To visualize cellular uptake, CDELNs were labeled with the Evlink 505 Exosome-Labeling Kit (EL012100200, Tianjin Exosome Technology Co., Ltd, China) and then incubated with TM4 cell for 12 h. .The cell membrane was stained with the Celllink 555 Cell Membrane-Labeling Kit (CL012100200, Tianjin Exosome Technology Co., Ltd, China), followed by cell fixation and nuclear counterstaining with DAPI. All fluorescent images were acquired using a confocal microscope (AXR, Nikon, Japan). To reveal the cellular uptake pathway of CDELNs, TM4 cells were pretreated with different endocytosis inhibitors[98,99], including 50 μM amiloride (HY-B0285A, MedChemExpress (MCE), USA), 50 μM indomethacin (HY-14397, MCE, USA), 50 μM Methyl-β-cyclodextrin (HY-101461, MCE, USA)(MβCD), 5 μM chlorpromazine (31679, Sigma, USA), or 50 μg/mL heparin (A5066, APExBIO, USA) at 37 °C for 2 h. Then DiD-labeled CDELNs were added for additional 4 h of co-incubation. Finally, cells were collected for flow cytometry analysis.

Cell viability assay

The cell viability was assayed by using 3-(4,5-dimethylthiazol-2-yl)-2,5-diphenyl tetrazolium bromide (MTT, M8180, Solarbio, China) method. Briefly, cells were plated in 96-well plates with 4,000 cells/well and treated with 4 μM 4-HC for 8 h for establishing cell injury model. Then, the cells were treated respectively with different conditions including CDELNs, miRNA mimic, P21 siRNA, *pCMV*6-p21, betaine (B105556, Aladdin, China), malic acid (DP0018, Desite, China) or choline (C875195, Macklin, China) for 24 h. Finally, 10% MTT were added and incubated with cells for 3 h. Absorbance was measured using a microplate reader (800TS, BioTek, USA).

Cell cycle analysis

Cells were gathered, rinsed three times with PBS, and preserved for 12 h in a 70% *v*/*v* cold ethanol solution. PI staining solution and RNase A solution (CA1510, Solarbio, China) were added and incubated with the cells for 30 min. The DNA contents were then measured using flow cytometry.

ROS measurement

TM4 cells were incubated with the fluorescent probe DCFH-DA (S1105S, Beyotime, China) at 37 ℃ for 30 min. The cells were collected and analyzed by flow cytometry. In addition, fluorescent images were obtained using an inverted fluorescence microscope (Olympus, Japan).

Immunofluorescence staining of γ-H2AX

Immunofluorescence detection of γ-H2AX was performed using the DNA Damage Assay Kit (C2035S, Beyotime, Shanghai, China). Samples were incubated with anti-γ-H2AX primary antibody, followed by washing with Immunol Staining Wash Buffer. Subsequently, cells were exposed to a fluorescein isothiocyanate under light-protected conditions. After nuclear counterstaining with DAPI, fluorescence images were captured.

Transient transfection

miRNA mimic (including miR858b, miR6300, miR168a-5p, and miR159b-3p mimics), miR159b-3p inhibitor, P21 siRNA, the total RNA or miRNA extracted from CDELNs, and the *pCMV*6-Entry vector carrying the coding sequences for full-length mouse P21 were respectively transfected into TM4 cells using Lipofectamine 3000 (L3000015, Thermo, USA) following the manufacturer's instructions.

Dual-luciferase assay

HEK293T cells were co-transfected with 0.5 μg of either wild-type or mutant P21 3'UTR cloned to SV40-firefly_Luciferase-MCS (GV272) and Tk promoter-luciferase hRluc (CV308) vector (Genechem, China), along with 30 nM miR159b-3p, using Lipofectamine 3000. After 24 h, luciferase activities were measured with a dual-luciferase reporter assay system (DL101-01, Vazyme, China). The firefly luciferase signal was normalized to that of Renilla luciferase for data analysis.

Biodistribution of CDELNs *in vivo*

CDELNs were stained with DiR (C11585, Psaitong, China) and then intraperitoneally injected into mice. After 2, 4, 8, 12, 24, 36, or 48 h, fluorescence signals were measured using the IVIS Spectrum system (PerkinElmer, USA). At 24 h post-administration,

serum samples were collected and the aforementioned organs were homogenized to prepare single-cell suspensions for fluorescence correlation spectroscopy (FCS) analysis. The experimental group received DiR-labeled CDELNs. The experimental setup for FCS was implemented in accordance with reference methods[100]. Data collection consisted of 10 recording cycles per sample, with each autocorrelation curve measured for 10 seconds.

Hemolysis assays

Erythrocytes were isolated from healthy mouse blood through sequential saline washes. The collected cells were then resuspended in saline to obtain a 2% (*v*/*v*) erythrocyte suspension. This suspension was combined with an equal volume of saline containing varying protein concentrations of CDELNs. For control groups, phosphate-buffered saline and 0.1% Triton X-100 (LS1394, Harveybio, China) were employed as negative and positive controls, respectively. Mixtures were all incubated at 37 °C for 3 h before centrifugation at 2000 rpm, and the absorbance at 541 nm was measured. The hemolysis rate was determined according to Eq.

$$\text{Hemolysis (\%)} = \frac{\text{OD}(CELNs) - \text{OD}(PBS)}{\text{OD}(Triton\ X - 100) - \text{OD}(PBS)} \times 100$$

Biosafety of CDELNs in *vivo*

To assess the biosafety of CDELNs, mice were randomly assigned to control group and CDELNs-treated group and received intraperitoneal injections of CDELNs (2.5 mg/kg/d) for two weeks. During the experiment period, body weight was measured every other day. After two weeks, tissue samples from the heart, liver, spleen, lung, kidney, and testis were collected for histological analysis. Serum levels of [alanine aminotransferase (ALT) (C009-3-2), aspartate transaminase (AST) (C010-3-1), albumin (ALB) (A028-1-1), uric acid (UA) (C012-1-1), and total serum protein (TP) (A045-2-2)] were measured using commercial assay kits from Nanjing Jiancheng. Haematological parameters were analyzed with a BC-5000Vet automated biochemical analyzer (Mindray Animal, China). For reproductive toxicity evaluation, bilateral testes were weighed and the left epididymal was dissected to assess sperm quality.

Sperm parameter testing

The left epididymis was isolated from each group of mice and placed in 1 mL of pre-warmed (37°C) HTF medium, after mincing and thorough mixing. A 20 μL aliquot of sperm-containing HTF medium was transferred to a glass slide for microscopic examination. CASA was performed using the SSA- II /PLUS system (SuiJia Software, China). The sperm motility rate was assessed in four to five randomly selected microscopic fields.

Enzyme-linked immunosorbent assay (ELISA)

Serum hormones were measured by ELISA kits (Beijing Feimo Biotechnology Co., Ltd., China). Briefly, samples and standard reagents were added to pre-coated microwell plates. Sequential incubations with biotin and enzyme-conjugated solutions were performed at 37°C. After adding chromogenic substrate, absorbance was measured at 450 nm using a microplate reader (800TS, BioTek, USA). Concentrations were calculated according to the standard curve equation.

Histological analysis

The tissues including heart, liver, spleen, lung, kidney and testis were harvested, rinsed in physiological saline, and immediately fixed in 4% paraformaldehyde at 4°C for 24 h. Following gradient ethanol dehydration and clearing, the tissues were embedded in paraffin and sectioned into 5 μm-thick slices. After dewaxing and rehydration, the sections were stained with hematoxylin and eosin (H&E), displaying dark blue nuclei and pink cytoplasm. The stained sections were examined using a light microscope (Nikon Eclipse ci, Japan) to evaluate morphological characteristics and pathological alterations in the tissues.

RNA fluorescence in situ hybridization (FISH)

The Cy3-labeled miR159b-3p probe was designed and synthesized by Servicebio Technology Co., Ltd. (China). The sequence of the probe is listed in Table S2. Following fixation, tissues were dehydrated, embedded in paraffin, and sectioned. The sections were then dehydrated with ethanol, followed by antigen retrieval and digestion. Pre-hybridization solution was applied, and the sections were incubated at 37°C for 1 h. Subsequently, the FISH probe (500 nM) was co-incubated with the sections at 40°C

overnight. After nuclear counterstaining with DAPI, fluorescence images were captured with the Nikon Eclipse CI ortho-fluorescent microscope (Nikon, Japan).

Immunofluorescence (IF)

Pre-cultured and fixed TM4 cells and paraffin sections were incubated with primary antibodies against P21 (1:5000/1:2000, 28248-1-1AP, Proteintech, China), CDK1 (1:4000/1:3000, 19532-1-AP, Proteintech, China), p-CDK1 (1:1000, AF8137, Affbiotech, China), ZO-1 (1:1000, 21773-1-AP, Proteintech, China), Occludin (1:1000, 27260-1-AP, Proteintech, China), or Claudin 1 (1:500, 28674-1-AP, Proteintech, China) at 4 °C overnight. Following PBS washes, samples were treated with species-appropriate horseradish peroxidase-conjugated secondary antibodies (anti-mouse or anti-rabbit) for 1 h at ambient temperature. After nuclear counterstaining with DAPI, fluorescence images were captured using an inverted fluorescence microscope (Olympus, Japan)..

Fertility assay

6- to 8-week-old male mice (Ctrl, *n*=6; CP group, *n*=6; TP group, *n*=6; CDELNs-L group, *n*=6; CDELNs-H group, *n*=6) were mated with 9- to 10-week-old female mice respectively at a 1:2 ratio and co-housed overnight. Vaginal smears were collected from female mice the next morning and examined microscopically. The presence of sperm in the smear was considered evidence of successful mating, and these females were subsequently housed separately. The number of pups per litter and pregnancy mice were recorded for statistical analysis.

Quantitative real-time PCR for RNA expression

For analysis of mRNA expression, total RNA was extracted from cells or testicular tissues using the FastPure® Cell/Tissue Total RNA Isolation Kit V2 (RC112-01, Vazyme, China). 500 ng of total RNA was reverse transcribed into cDNA using HiScript® III All-in-one RT SuperMix Perfect for qPCR (R333-01, Vazyme, China). Real-time PCR amplification was performed on an MXPro3005P Cycler (Agilent Technology, Germany) with Taq Pro Universal SYBR qPCR Master Mix (Q712-02, Vazyme, China) and the listed primers (Supplementary Table1). Relative mRNA

expression levels normalized to β-actin were calculated using the $2^{-\Delta\Delta Ct}$ method.

For analysis of miRNA expression, total RNA was polyadenylated at the 3' end using Poly A polymerase (PAP) from the miRNA 1st Strand cDNA Synthesis Kit (by tailing A) (MR201-02, Vazyme, China), followed by reverse transcription with universal primers. Quantitative PCR was carried out on the MXPro3005P system (Agilent Technologies, Germany) using the miRNA Unimodal SYBR qPCR Master Mix (MQ102-02, Vazyme, China) and the listed primers (Supplementary Table 2). Relative miRNA expression levels normalized to U6 were calculated using the $2^{-\Delta\Delta Ct}$ method.

Western blot analysis

Testicular tissues and cells were lysed in ice-cold RIPA buffer (C1053, Feimobio, China) supplemented with protease and phosphatase inhibitor cocktail (HY-K0013, MCE, USA). Proteins were separated on 10% SDS–PAGE gelsand electrotransferred onto PVDF membranes (PVDF045, CobBio, China). The PVDF membranes were blocked with 5% nonfat powdered milk and incubated with specific primary and secondary antibodies. Signal detection was performed with ECL (BF06053, Biodragon, China) method using the Tanon-5200 imaging system (Bio-Tanon, China). Protein band intensities were quantified via ImageJ software with normalization to GAPDH or β-Tubulin for relative expression analysis. Primary antibodies included anti-P21 (1:2000, 28248-1-1AP, Proteintech, China), anti-CDK1 (1:3000, 19532-1-AP, Proteintech, China), anti-phos-CDK1 (1:1000, AF8137, Affbiotech, China), anti-GAPDH (1:5000, 10494-1-AP, Proteintech, China), and anti-β-Tublin (1:2000, 10094-1-AP, Proteintech, China). Secondary antibodies included HRP-conjugated Goat Anti-Rabbit/Anti-Mouse IgG(H+L) (1:5000, SA00001-2/SA00001-1, Proteintech, China).

Online data analysis

Using the Singleron CeleLens cloud platform (https://cn.singleronbio.com/), differential expression analysis of P21 in testicular tissues from healthy individuals and patients with non-obstructive azoospermia (NOA) was performed, with data sourced from GEO (GSE149512).

Statistical analysis

Statistical analysis was performed using GraphPad Prism (9.3.0 version, USA), with all measurements presented as mean ± SDs. Differences between groups were assessed by one-way ANOVA or unpaired Student's t-test as appropriate, with $p < 0.05$ defined as statistically significant. Detailed statistical parameters and specific sample sizes are provided in the corresponding figure legends.

Data availability

All data supporting the conclusions of this study are presented in the article and the Supplementary Information. Source Data are provided in this paper. Source data are provided in this paper.

References

1. Finkelstein, J. S. *et al.* Gonadal Steroids and Body Composition, Strength, and Sexual Function in Men. *N. Engl. J. Med.* **369**, 1011–1022 (2013).
2. Oatley, J. M. & Brinster, R. L. The germline stem cell niche unit in mammalian testes. *Physiol. Rev.* **92**, 577–595 (2012).
3. Sung, H. *et al.* Global Cancer Statistics 2020: GLOBOCAN Estimates of Incidence and Mortality Worldwide for 36 Cancers in 185 Countries. *CA. Cancer J. Clin.* **71**, 209–249 (2021).
4. Benson, A. J. *et al.* N-(2-hydroxyethyl)-N-[2-(7-guaninyl)ethyl]amine, the putative major DNA adduct of cyclophosphamide in vitro and in vivo in the rat. *Biochem. Pharmacol.* **37**, 2979–2985 (1988).
5. Elangovan, N., Chiou, T.-J., Tzeng, W.-F. & Chu, S.-T. Cyclophosphamide treatment causes impairment of sperm and its fertilizing ability in mice. *Toxicology* **222**, 60–70 (2006).
6. Kim, W., Kim, S.-H., Park, S. K. & Chang, M. S. Astragalus membranaceus Ameliorates Reproductive Toxicity Induced by Cyclophosphamide in Male Mice. *Phytother. Res.* **26**, 1418–1421 (2012).
7. Le, X. Y., Luo, P., Gu, Y. P., Tao, Y. X. & Liu, H. Z. Interventional effects of squid ink polysaccharides on cyclophosphamide-associated testicular damage in mice. *Bratisl. Med. J.* **116**, 334–339 (2015).
8. Nayak, G. *et al.* Ethanolic extract of Moringa oleifera leaves alleviate cyclophosphamide-induced testicular toxicity by improving endocrine function and modulating cell specific gene expression in mouse testis. *J. Ethnopharmacol.* **259**, 112922 (2020).
9. AbuMadighem, A., Cohen, O. & Huleihel, M. Elucidating the Transcriptional States of Spermatogenesis-Joint Analysis of Germline and Supporting Cell, Mice and Human, Normal and Perturbed, Bulk and Single-Cell RNA-Seq. *Biomolecules* **14**, 840 (2024).

10. Ghobadi, E., Moloudizargari, M., Asghari, M. H. & Abdollahi, M. The mechanisms of cyclophosphamide-induced testicular toxicity and the protective agents. *Expert Opin. Drug Metab. Toxicol.* **13**, 525–536 (2017).
11. Özbilgin, M. K., Demirören, S., Üçöz, M. & Oztatlici, M. Cyclophosphamide suppresses spermatogenesis in the testis of mice through downregulation of miR-34b and miR-34c. *Andrologia* **53**, e14071 (2021).
12. Gao, Y. *et al.* Unveiling the roles of Sertoli cells lineage differentiation in reproductive development and disorders: a review. *Front. Endocrinol.* **15**, 1357594 (2024).
13. Boekelheide, K. Mechanisms of Toxic Damage to Spermatogenesis. *JNCI Monogr.* **2005**, 6–8 (2005).
14. Barrionuevo, F., Burgos, M. & Jiménez, R. Origin and function of embryonic Sertoli cells. **2**, 537–547 (2011).
15. Feng, Y., Fang, X., Shi, Z., Xu, M. & Dai, J. Effects of PFNA exposure on expression of junction-associated molecules and secretory function in rat Sertoli cells. *Reprod. Toxicol. Elmsford N* **30**, 429–437 (2010).
16. Shubin, A. V., Demidyuk, I. V., Komissarov, A. A., Rafieva, L. M. & Kostrov, S. V. Cytoplasmic vacuolization in cell death and survival. *Oncotarget* **7**, 55863–55889 (2016).
17. Zhao, D. *et al.* Polygonatum sibiricum Saponin Prevents Immune Dysfunction and Strengthens Intestinal Mucosal Barrier Function in Cyclophosphamide-Induced Immunosuppressed BALB/c Mice. *Foods* **13**, 934 (2024).
18. Kalluri, R. & LeBleu, V. S. The biology, function, and biomedical applications of exosomes. *Science* **367**, eaau6977 (2020).
19. Cocozza, F., Grisard, E., Martin-Jaular, L., Mathieu, M. & Théry, C. SnapShot: Extracellular Vesicles. *Cell* **182**, 262-262.e1 (2020).
20. Hendrix, A. *et al.* Extracellular vesicle analysis. *Nat. Rev. Methods Primer* **3**, 56 (2023).
21. Mu, N. *et al.* Plant-Derived Exosome-Like Nanovesicles: Current Progress and Prospects. *Int. J. Nanomedicine* **Volume 18**, 4987–5009 (2023).
22. Zhao, B. *et al.* Exosome-like nanoparticles derived from fruits, vegetables, and herbs: innovative strategies of therapeutic and drug delivery. *Theranostics* **14**, 4598–4621 (2024).
23. Seo, K. *et al.* Ginseng-derived exosome-like nanovesicles extracted by sucrose gradient ultracentrifugation to inhibit osteoclast differentiation. *Nanoscale* **15**, 5798–5808 (2023).
24. Feng, Z. *et al.* Medicinal Plant-Derived Exosome-Like Nanovesicles as Regulatory Mediators in Microenvironment for Disease Treatment. *Int. J. Nanomedicine* **Volume 20**, 8451–8479 (2025).
25. Fu, J. *et al.* Platycodon grandiflorum exosome-like nanoparticles: the material basis of fresh platycodon grandiflorum optimality and its mechanism in regulating acute lung injury. *J. Nanobiotechnology* **23**, 270 (2025).
26. Li, D. *et al.* Plant-derived exosomal nanoparticles: potential therapeutic for inflammatory bowel disease. *Nanoscale Adv.* **5**, 3575–3588.
27. Volpini, L., Monaco, F., Santarelli, L., Neuzil, J. & Tomasetti, M. Advances in RNA cancer therapeutics: New insight into exosomes as miRNA delivery. *Asp. Mol. Med.* **1**, 100005 (2023).
28. Sundaram, K. *et al.* Plant-Derived Exosomal Nanoparticles Inhibit Pathogenicity of Porphyromonas gingivalis. *iScience* **21**, 308–327 (2019).

29. Akao, Y. *et al.* Plant hvu-MIR168-3p enhances expression of glucose transporter 1 (SLC2A1) in human cells by silencing genes related to mitochondrial electron transport chain complex I. *J. Nutr. Biochem.* **101**, 108922 (2022).
30. Liu, X. *et al.* Bioactive Components, Pharmacological Properties, and Applications of Cistanche deserticola Y. C. Ma: A Comprehensive Review. *Nutrients* **17**, 1501 (2025).
31. Song, Y., Zeng, K., Jiang, Y. & Tu, P. Cistanches Herba, from an endangered species to a big brand of Chinese medicine. *Med. Res. Rev.* **41**, 1539–1577 (2021).
32. Lei, H. *et al.* Herba Cistanche (Rou Cong Rong): A Review of Its Phytochemistry and Pharmacology. *Chem. Pharm. Bull. (Tokyo)* **68**, 694–712 (2020).
33. Bi, Y. *et al.* Therapeutic, nutritional benefits, and applications of Cistanche Deserticola Y.C.Ma: a systematic review. *Food Nutr. Health* **2**, 24 (2025).
34. Tian, X.-Y. *et al.* A review on the structure and pharmacological activity of phenylethanoid glycosides. *Eur. J. Med. Chem.* **209**, 112563 (2021).
35. Delgado, A. V., González-Caballero, F., Hunter, R. J., Koopal, L. K. & Lyklema, J. Measurement and interpretation of electrokinetic phenomena. *J. Colloid Interface Sci.* **309**, 194–224 (2007).
36. Dad, H. A., Gu, T.-W., Zhu, A.-Q., Huang, L.-Q. & Peng, L.-H. Plant Exosome-like Nanovesicles: Emerging Therapeutics and Drug Delivery Nanoplatforms. *Mol. Ther.* **29**, 13–31 (2021).
37. Wang, T. *et al.* Cistanche tubulosa ethanol extract mediates rat sex hormone levels by induction of testicular steroidgenic enzymes. *Pharm. Biol.* **54**, 481–487 (2016).
38. Wang, Q. *et al.* Phenylethanol glycosides from Cistanche tubulosa improved reproductive dysfunction by regulating testicular steroids through CYP450-3β-HSD pathway. *J. Ethnopharmacol.* **251**, 112500 (2020).
39. Zhukov, A. & Vereshchagin, M. Polar Glycerolipids and Membrane Lipid Rafts. *Int. J. Mol. Sci.* **25**, 8325 (2024).
40. Kang, J.-H., Toita, R., Kawano, T., Murata, M. & Kano, A. Phospholipids and their metabolites as diagnostic biomarkers of human diseases. *Prog. Lipid Res.* **99**, 101340 (2025).
41. Abdulmalek, O. A. A. Y. *et al.* Therapeutic Applications of Stem Cell-Derived Exosomes. *Int. J. Mol. Sci.* **25**, 3562 (2024).
42. Giepmans, B. N. G. Gap junctions and connexin-interacting proteins. *Cardiovasc. Res.* **62**, 233–245 (2004).
43. Hervé, J.-C., Bourmeyster, N., Sarrouilhe, D. & Duffy, H. S. Gap junctional complexes: from partners to functions. *Prog. Biophys. Mol. Biol.* **94**, 29–65 (2007).
44. Strauss, R. E. & Gourdie, R. G. Cx43 and the Actin Cytoskeleton: Novel Roles and Implications for Cell-Cell Junction-Based Barrier Function Regulation. *Biomolecules* **10**, 1656 (2020).
45. He, S. *et al.* High-density lipoprotein nanoparticles spontaneously target to damaged renal tubules and alleviate renal fibrosis by remodeling the fibrotic niches. *Nat. Commun.* **16**, 1061 (2025).
46. Zhang, Z.-A. *et al.* Novel brain-targeted nanomicelles for anti-glioma therapy mediated by the ApoE-enriched protein corona in vivo. *J. Nanobiotechnology* **19**, 453 (2021).
47. Idowu, E. T., Alimba, C. G., Olowu, E. A. & Otubanjo, A. O. Artemether-Lumefantrine

treatment combined with albendazole and ivermectin induced genotoxicity and hepatotoxicity through oxidative stress in Wistar rats. *Egypt. J. Basic Appl. Sci.* **2**, 110–119 (2015).
48. Trujillo, M., Odle, A. K., Aykin-Burns, N. & Allen, A. R. Chemotherapy induced oxidative stress in the ovary: drug-dependent mechanisms and potential interventions†. *Biol. Reprod.* **108**, 522–537 (2023).
49. Al Bitar, S. & Gali-Muhtasib, H. The Role of the Cyclin Dependent Kinase Inhibitor p21cip1/waf1 in Targeting Cancer: Molecular Mechanisms and Novel Therapeutics. *Cancers* **11**, 1475 (2019).
50. Cai, Q. *et al.* Plants send small RNAs in extracellular vesicles to fungal pathogen to silence virulence genes. *Science* **360**, 1126–1129 (2018).
51. Yang, Y. *et al.* Coptis chinensis-derived extracellular vesicle-like nanoparticles delivered miRNA-5106 suppresses NETs by restoring zinc homeostasis to alleviate colitis. *J. Nanobiotechnology* **23**, 444 (2025).
52. Lv, Q. *et al.* Prunus mume derived extracellular vesicle-like particles alleviate experimental colitis via disrupting NEK7-NLRP3 interaction and inflammasome activation. *J. Nanobiotechnology* **23**, 532 (2025).
53. Starega-Roslan, J., Galka-Marciniak, P. & Krzyzosiak, W. J. Nucleotide sequence of miRNA precursor contributes to cleavage site selection by Dicer. *Nucleic Acids Res.* **43**, 10939–10951 (2015).
54. Ye, J. *et al.* Integration of Transcriptomes, Small RNAs, and Degradome Sequencing to Identify Putative miRNAs and Their Targets Related to Eu-Rubber Biosynthesis in Eucommia ulmoides. *Genes* **10**, 623 (2019).
55. Malumbres, M. & Barbacid, M. Cell cycle, CDKs and cancer: a changing paradigm. *Nat. Rev. Cancer* **9**, 153–166 (2009).
56. King, K. L. & Cidlowski, J. A. Cell cycle regulation and apoptosis. *Annu. Rev. Physiol.* **60**, 601–617 (1998).
57. Witika, B. A. *et al.* Biocompatibility of Biomaterials for Nanoencapsulation: Current Approaches. *Nanomaterials* **10**, 1649 (2020).
58. Yang, M. *et al.* Platycodon grandiflorum-derived extracellular vesicles suppress triple-negative breast cancer growth by reversing the immunosuppressive tumor microenvironment and modulating the gut microbiota. *J. Nanobiotechnology* **23**, 92 (2025).
59. Cheng, C. Y. & Mruk, D. D. A local autocrine axis in the testes that regulates spermatogenesis. *Nat. Rev. Endocrinol.* **6**, 380–395 (2010).
60. Kaur, G., Thompson, L. A. & Dufour, J. M. Sertoli cells- Immunological sentinels of spermatogenesis. *Semin. Cell Dev. Biol.* **0**, 36–44 (2014).
61. Garcia, J. G. N. Concepts in microvascular endothelial barrier regulation in health and disease. *Microvasc. Res.* **77**, 1–3 (2009).
62. Payne, L. B., Hoque, M., Houk, C., Darden, J. & Chappell, J. C. Pericytes in Vascular Development. *Curr. Tissue Microenviron. Rep.* **1**, 143–154 (2020).
63. Bennett, C. *et al.* Neuroinflammation, oxidative stress, and blood-brain barrier (BBB) disruption in acute Utah electrode array implants and the effect of deferoxamine as an iron chelator on acute foreign body response. *Biomaterials* **188**, 144–159 (2019).

64. Zhang, C., Liu, J., Wang, J., Zhang, T. & Feng, Z. The Interplay Between Tumor Suppressor p53 and Hypoxia Signaling Pathways in Cancer. *Front. Cell Dev. Biol.* **9**, (2021).
65. Brosh, R. *et al.* p53-dependent transcriptional regulation of EDA2R and its involvement in chemotherapy-induced hair loss. *FEBS Lett.* **584**, 2473–2477 (2010).
66. Hubbard, L., Rambhatla, A. & Glina, S. Nonobstructive azoospermia: an etiologic review. *Asian J. Androl.* **27**, 279–287 (2024).
67. Kobori, Y. Home testing for male factor infertility: a review of current options. *Fertil. Steril.* **111**, 864–870 (2019).
68. Hamada, A. J., Esteves, S. C. & Agarwal, A. A comprehensive review of genetics and genetic testing in azoospermia. *Clinics* **68**, 39–60 (2013).
69. Esteves, S. C. Clinical management of infertile men with nonobstructive azoospermia. *Asian J. Androl.* **17**, 459–470 (2015).
70. Campbell, K. *et al.* Next Generation Sequencing Analysis of Semen Microbiome Taxonomy in Men with Non-Obstructive Azoospermia vs Fertile Controls: a Pilot Study. *FS Sci.* **4**, 257–264 (2023).
71. Cocuzza, M., Alvarenga, C. & Pagani, R. The epidemiology and etiology of azoospermia. *Clinics* **68**, 15–26 (2013).
72. Fakhro, K. A. *et al.* Point-of-care whole-exome sequencing of idiopathic male infertility. *Genet. Med. Off. J. Am. Coll. Med. Genet.* **20**, 1365–1373 (2018).
73. Zhao, L. *et al.* Single-cell analysis of developing and azoospermia human testicles reveals central role of Sertoli cells. *Nat. Commun.* **11**, 5683 (2020).
74. Lu, W.-H. & Gu, Y.-Q. Insights into semen analysis: a Chinese perspective on the fifth edition of the WHO laboratory manual for the examination and processing of human semen. *Asian J. Androl.* **12**, 605–606 (2010).
75. Mai, Z. *et al.* A narrative review of mitochondrial dysfunction and male infertility. *Transl. Androl. Urol.* **13**, 2134–2145 (2024).
76. Agarwal, A. *et al.* Male infertility. *The Lancet* **397**, 319–333 (2021).
77. Babakhanzadeh, E., Nazari, M., Ghasemifar, S. & Khodadadian, A. Some of the Factors Involved in Male Infertility: A Prospective Review. *Int. J. Gen. Med.* **13**, 29–41 (2020).
78. Gajjar, R., Miller, S. D., Meyers, K. E. & Ginsberg, J. P. Fertility preservation in patients receiving cyclophosphamide therapy for renal disease. *Pediatr. Nephrol.* **30**, 1099–1106 (2015).
79. Kenney, L. B., Laufer, M. R., Grant, F. D., Grier, H. & Diller, L. High risk of infertility and long term gonadal damage in males treated with high dose cyclophosphamide for sarcoma during childhood. *Cancer* **91**, 613–621 (2001).
80. Kaltsas, A. Oxidative Stress and Male Infertility: The Protective Role of Antioxidants. *Medicina (Mex.)* **59**, 1769 (2023).
81. Kumar Netam, A., Pankaj Bhargava, V., Singh, R. & Sharma, P. Testosterone propionate and Swarna Bhasma treatment modulated D-galactose induced reproductive alterations in male Wistar rats: An experimental study. *Int. J. Reprod. Biomed.* **21**, 303–322 (2023).
82. Segunda, M. N. *et al.* Potential of mesenchymal stromal/stem cells and spermatogonial stem cells for survival and colonization in bull recipient testes after allogenic transplantation. *Theriogenology* **230**, 192–202 (2024).

83. Irani, D., Mehrabani, D. & KarimiBusheri, F. Mesenchymal Stem Cells in Regenerative Medicine Possible Applications in The Restoration of Spermatogenesis: A Review. *Cell J. Yakhteh* **26**, (2024).
84. Pan, Z. *et al.* Protective Effects of Selenium Nanoparticles against Bisphenol A-Induced Toxicity in Porcine Intestinal Epithelial Cells. *Int. J. Mol. Sci.* **24**, 7242 (2023).
85. Dkhil, M. A., Zrieq, R., Al-Quraishy, S. & Abdel Moneim, A. E. Selenium Nanoparticles Attenuate Oxidative Stress and Testicular Damage in Streptozotocin-Induced Diabetic Rats. *Molecules* **21**, 1517 (2016).
86. Mu, J. *et al.* Interspecies communication between plant and mouse gut host cells through edible plant derived exosome-like nanoparticles. *Mol. Nutr. Food Res.* **58**, 1561–1573 (2014).
87. Zhang, M. *et al.* Oral administration of Sophora Flavescens-derived exosomes-like nanovesicles carrying CX5461 ameliorates DSS-induced colitis in mice. *J. Nanobiotechnology* **22**, 607 (2024).
88. Tembo, K. M. *et al.* Exploring the bioactivity of MicroRNAs Originated from Plant-derived Exosome-like Nanoparticles (PELNs): current perspectives. *J. Nanobiotechnology* **23**, 563 (2025).
89. Teng, Y. *et al.* Plant-Derived Exosomal MicroRNAs Shape the Gut Microbiota. *Cell Host Microbe* **24**, 637-652.e8 (2018).
90. Yan, G. *et al.* Brucea javanica derived exosome-like nanovesicles deliver miRNAs for cancer therapy. *J. Controlled Release* **367**, 425–440 (2024).
91. Yan, F. *et al.* Cistanoside of Cistanche Herba ameliorates hypoxia-induced male reproductive damage via suppression of oxidative stress. *Am. J. Transl. Res.* **13**, 4342–4359 (2021).
92. Shen, J.-Y., Yang, X.-L., Yang, Z.-L., Kou, J.-P. & Li, F. Enhancement of absorption and bioavailability of echinacoside by verapamil or clove oil. *Drug Des. Devel. Ther.* **9**, 4685–4693 (2015).
93. O'Donnell, L., Smith, L. B. & Rebourcet, D. Sertoli cells as key drivers of testis function. *Semin. Cell Dev. Biol.* **121**, 2–9 (2022).
94. Huang, C.-C. *et al.* Metformin: a novel promising option for fertility preservation during cyclophosphamide-based chemotherapy. *Mol. Hum. Reprod.* **27**, gaaa084 (2021).
95. Chang, B.-D. *et al.* Role of p53 and p21waf1/cip1 in senescence-like terminal proliferation arrest induced in human tumor cells by chemotherapeutic drugs. *Oncogene* **18**, 4808–4818 (1999).
96. Bodzak, E., Blough, M. D., Lee, P. W. K. & Hill, R. p53 binding to the p21 promoter is dependent on the nature of DNA damage. *Cell Cycle* **7**, 2535–2543 (2008).
97. Song, Y. *et al.* An integrated strategy to quantitatively differentiate chemome between *Cistanche deserticola* and *C. tubulosa* using high performance liquid chromatography–hybrid triple quadrupole-linear ion trap mass spectrometry. *J. Chromatogr. A* **1429**, 238–247 (2016).
98. Yin, L. *et al.* Characterization of the MicroRNA Profile of Ginger Exosome-like Nanoparticles and Their Anti-Inflammatory Effects in Intestinal Caco-2 Cells. *J. Agric. Food Chem.* **70**, 4725–4734 (2022).
99. Fu, J. *et al.* Absorption and transport mechanism of colloidal nanoparticles (CNPs) in lamb

soup based on Caco-2 cell. *Food Chem.* **463**, 141196 (2025).
100. Zhang, M. *et al.* Phosphorylation-dependent charge blocks regulate the relaxation of nuclear speckle networks. *Mol. Cell* **85**, 1760-1774.e7 (2025).

Acknowledgements

This work was supported by the National Natural Science Foundation of China (82104543, U23A20514, Y.J.), Beijing Natural Science Foundation-Daxing Innovation Joint Fund (2025DXPY043, Y.J.), the National Natural Science Foundation of China (82402488, X.Z.), and the Key Research and Development Project of Xinjiang (2022B02012, 2022E02122, Y.J.).

Author Contributions

Y. J. and X. Z. designed the study. Y.L.X., C.L.W., M. D. and W.X.T. performed the experiments. Y.L.X. and X.Z.H. performed bioinformatics analysis of single-cell RNA sequencing. Y. J. and P.F.T. provided *Cistanche deserticola* resources. Y. J. supervised the project. Y. J., X. Z., and Y.L.X. wrote the manuscript. All authors helped with data interpretation and manuscript reviewing.

Competing interests

The authors declare no competing interests.

Additional information

Supplementary information The online version contains supplementary material.

Correspondence and requests for materials should be addressed to Yong Jiang or Xiao Zhang.

Supplementary Files

This is a list of supplementary files associated with this preprint. Click to download.

- SupplementaryMaterials.pdf